

A New Method for Determining Cumulative Gravitational Lensing Effects in Inhomogeneous Universes

Daniel E. Holz and Robert M. Wald
Enrico Fermi Institute and Department of Physics
University of Chicago
5640 S. Ellis Avenue
Chicago, Illinois 60637-1433

November 26, 2024

Abstract

We present a new approach to calculating the statistical distributions for magnification, shear, and rotation of images of cosmological sources due to gravitational lensing. In this approach one specifies an underlying Robertson-Walker cosmological model together with relevant information on the clumping of matter on scales much smaller than the Hubble radius. The geodesic deviation equation is then integrated backwards in time until the desired redshift is reached, using a Monte Carlo procedure wherein each photon beam in effect “creates its own universe” as it propagates. The approach is somewhat similar to that used in “Swiss cheese” models, but the “cheese” has been completely eliminated, the matter distribution in the “voids” need not be spherically symmetric, the total mass in each void need equal the corresponding Robertson-Walker mass only on average, and we do not impose an “opaque radius” cutoff. The case where the matter in the universe consists of point masses is studied in detail, and it is shown that the statistical distributions of the lensing images are essentially independent of both the mass spectrum and the clustering properties of the point masses, provided that the clustering is spherical. Detailed results for the distribution of the magnification of images are

presented for the point mass case, as well as a number of other matter distributions. We apply our results (i) to argue that the positive correlation recently found between quasar luminosity and the number of absorption line systems is not likely to be due to lensing, and (ii) to determine the amount of “noise” and possible bias produced by lensing in measurements of q_0 using distant supernovae.

1 Introduction

In recent years there has been a great deal of interest in studying the effects on cosmologically distant sources produced by gravitational lensing due to intervening matter. In many cases of interest, the lensing effects can be assumed to be produced by a single galaxy or cluster of galaxies, and one can use the detailed structure of the images produced by lensing to extract a great deal of information about the mass distribution of the galaxy or cluster. However, in other circumstances of interest one may be interested in the cumulative lensing effects produced by many different objects (or voids), and one may be primarily interested in statistical distributions of the image brightenings and/or distortions, rather than the detailed modeling of any individual lens system.

Two examples of the latter circumstances are the following: (1) Vanden Berk *et al.* [1] have presented evidence for a positive correlation between quasar luminosity and the number of intervening Carbon IV absorption clouds. Could this correlation be the result of the cumulative gravitational lensing effects produced by the mass distributions associated with these clouds? (2) Efforts are currently underway to use supernovae occurring at cosmological distances as standard candles for tests of q_0 [2]. How much “noise” in the apparent luminosity distribution of the supernovae would be expected from gravitational lensing effects? Could any useful information about the distribution of matter in the universe be extractable from this “noise”?

The main purpose of this paper is to present a new approach for determining cumulative gravitational lensing effects on cosmological scales due to inhomogeneities in the matter distribution of the universe. As explained further below, in this approach one specifies an underlying Robertson-Walker cosmological model together with one’s assumptions concerning the detailed clumping and clustering of matter in the universe. Both the Robertson-

Walker model and the clumping/clustering of matter may be specified arbitrarily, provided that the clustering of matter occurs only on scales much smaller than the Hubble radius and that the average density of the matter distribution corresponds to that of the underlying Robertson-Walker model. Our approach then enables one to accurately obtain statistical distributions for the luminosity, shear, and rotation of images of “standard candle” (nearly) point sources at any cosmological redshift. When multiple images occur, however, even statistical information about the number of images and the relationships between the images cannot be easily extracted using our approach, since that would require us to keep track of the relationship between finitely (as opposed to infinitesimally) separated null geodesics. Nevertheless, statistical information about the luminosity, shear, and rotation of the individual images occurring in multiple images is included in our distributions.

The rest of this section will be devoted to an overview of our approach for determining statistical lensing effects in inhomogeneous universes. Subsection 1.1 introduces our cosmological model, presenting and justifying the metric which provides the framework for our results. Subsection 1.2 discusses lensing effects on the propagation of photon beams within the cosmology, while Subsection 1.3 discusses the local nature of these effects. Subsection 1.4 gives a general overview of our method, and Subsection 1.5 discusses the relevant scales of the model. In Section 2 we present our procedure for calculating statistical lensing effects in more explicit detail. In Section 3 we analyze the case where all of the matter in the universe can be treated as being comprised of point masses (satisfying Eq. (25)). Other distributions of mass are considered in Subsection 4.1, and then in Subsection 4.2 we perform some consistency checks on our results. Applications of our work to the analysis of lensing effects by quasar absorption systems are given in Section 5, and applications to the effects of lensing on supernovae luminosity are given in Section 6.

1.1 Cosmological Model

To explain our approach, we first need to state our cosmological assumptions with more precision. We assume that the spacetime metric of the universe is globally well approximated (on *all* scales) by a “Newtonianly perturbed Robertson-Walker metric” of the form

$$ds^2 = -(1 + 2\phi) d\tau^2 + (1 - 2\phi)a^2(\tau) \left[\frac{dr^2}{1 - kr^2} + r^2(d\theta^2 + \sin^2\theta d\varphi^2) \right], \quad (1)$$

where $k = 0, \pm 1$. We shall refer to the metric obtained by setting $\phi = 0$ in Eq. (1) as the *underlying Robertson-Walker model*. The spatial metric of this underlying Robertson-Walker model is $a^2 h_{ab}$, where

$$h_{ab} \equiv \frac{1}{1 - kr^2} dr_a dr_b + r^2 (d\theta_a d\theta_b + \sin^2 \theta d\varphi_a d\varphi_b) \quad (2)$$

is either the metric of a unit 3-sphere ($k = 1$), a unit 3-hyperboloid ($k = -1$), or flat 3-space ($k = 0$).

Without loss of generality, we may assume that the spatial average of ϕ vanishes, since a spatially constant part of ϕ could be absorbed into the definitions of τ and a . We also assume that throughout spacetime—or at least out to distance scales of order R_H , where $R_H \equiv H^{-1} = a/\dot{a}$ denotes the Hubble radius of the underlying Robertson-Walker model—we have

$$|\phi| \ll 1. \quad (3)$$

We further assume that time derivatives of ϕ are much smaller than spatial derivatives, i.e.,

$$|\partial\phi/\partial\tau|^2 \ll a^{-2} h^{ab} D_a \phi D_b \phi, \quad (4)$$

with similar relations holding for the higher time derivatives. Here D_a denotes the spatial derivative operator associated with h_{ab} , and h^{ab} denotes the inverse of h_{ab} (so $a^{-2} h^{ab}$ is the inverse spatial metric of the underlying Robertson-Walker model). It is important to note that spatial derivatives of ϕ may locally be very large compared with scales set by the underlying Robertson-Walker model. However, we assume that products of first spatial derivatives of ϕ are small compared with second derivatives, i.e.,

$$(h^{ab} D_a \phi D_b \phi)^2 \ll h^{ac} h^{bd} D_a D_b \phi D_c D_d \phi. \quad (5)$$

Finally, we assume that the matter stress-energy tensor, T_{ab} (*not* including the cosmological constant term), is everywhere such that, in the rest frame of the underlying Robertson-Walker model, the energy density of matter greatly dominates the other components of T_{ab} . In this case T_{ab} is approximately of the “matter dominated” form

$$T_{ab} \approx \rho u_a u_b, \quad (6)$$

where u^a is the unit (in the metric of Eq. (1)) timelike vector field orthogonal to the surfaces of constant τ . Eqs. (3)–(6) are the only assumptions we shall

need to obtain eqs. (9)–(11) below.¹ However, in Subsection 1.3 we shall also assume that there is a (co-moving) scale $\mathcal{R} \ll R_H$ such that no strong correlations in the density of matter occur on scales greater than \mathcal{R} .

We now substitute the metric form of Eq. (1) and the matter stress-energy of Eq. (6) into Einstein’s equation, possibly with a nonvanishing cosmological constant, Λ . We make the approximations of Eqs. (3)–(6), and also drop all terms (like $\Lambda\phi$ and $\rho\phi$) which are small compared with the curvature of the underlying Robertson-Walker metric. The nonvanishing components of Einstein’s equation then yield²

$$3\ddot{a}/a = \Lambda - 4\pi\rho + a^{-2}h^{ab}D_aD_b\phi \quad (7)$$

$$3(\dot{a}/a)^2 = \Lambda + 8\pi\rho - 2a^{-2}h^{ab}D_aD_b\phi - 3k/a^2, \quad (8)$$

where the dots denote derivatives with respect to τ . The spatial average of these equations yields the usual form of the matter dominated Einstein equations for the underlying Robertson-Walker metric, namely

$$3\ddot{a}/a = \Lambda - 4\pi\bar{\rho} \quad (9)$$

$$3(\dot{a}/a)^2 = \Lambda + 8\pi\bar{\rho} - 3k/a^2, \quad (10)$$

where $\bar{\rho}$ denotes the spatial average of ρ . Subtracting Eqs. (9) and (10) from Eqs. (7) and (8), we find the remaining content of Einstein’s equation is that

¹ E. Linder (private communication) has claimed that the approximation $\epsilon^2/\kappa \ll 1$ of references [3], [4], and [5] is also needed for the validity of our equations below. We do not agree with this claim.

²In addition to the two equations given here—which correspond to the time-time and diagonal space-space components of Einstein’s equation—there are also contributions to the time-space components of Einstein’s equation of the form ρv_a (where v_a denotes the velocity of the matter relative to the Hubble flow), $(\dot{a}/a)D_a\phi$, and mixed time-space derivatives of ϕ . These terms need not everywhere be small compared with the curvature of the underlying Robertson-Walker metric. If only these terms were considered, the time-space components of Einstein’s equation would yield additional equations for ϕ which would be inconsistent with Eq. (11) below. This difficulty is resolved by allowing for the presence of nonvanishing time-space components of the metric, $g_{0\mu}$ (with $\mu = 1, 2, 3$), satisfying $|g_{0\mu}| \ll |\phi|$. The time-space components of Einstein’s equation then become, in essence, equations which determine $g_{0\mu}$ (see Sec. 4.4a of [6] for further details in the ordinary Newtonian case). However, since $g_{0\mu}$ makes a negligible correction to the effects calculated in this paper, we shall ignore its presence below and, correspondingly, will not consider the time-space components of Einstein’s equation.

ϕ satisfies the Poisson equation³

$$a^{-2}h^{ab}D_aD_b\phi = 4\pi\delta\rho, \quad (11)$$

where

$$\delta\rho \equiv \rho - \bar{\rho}. \quad (12)$$

We emphasize that it is completely consistent with our assumptions to have, locally, $\delta\rho \gg \bar{\rho}$. It is essential that this be allowed if Eq. (1), together with Eqs. (3)–(5), are intended as an accurate description of our universe, since we commonly find $\delta\rho \sim 10^{30}\bar{\rho}$ in our vicinity.

Thus, in our model the matter is assumed to have an energy density much greater than its stresses, and is assumed to move non-relativistically with respect to the Hubble flow defined by the underlying Robertson-Walker model. However, unlike a Robertson-Walker model, this matter may be distributed in a very inhomogeneous manner; in particular, as already noted, the fluctuations in the mass density may be very large compared with the spatial average of the mass density. Consequently, the local curvature of spacetime may differ drastically from that of a Robertson-Walker model. Nevertheless, in our cosmological model, the Hubble flow of the matter and the causal structure of spacetime correspond very closely to the underlying matter dominated Robertson-Walker model, whose mass density is equal to the average density of matter in the universe.

It is useful to examine the form taken by the metric of Eq. (1) in a locally Minkowskian frame associated with an observer moving with the Hubble

³ Nonlinear terms in ϕ , such as $a^{-2}h^{ab}D_a\phi D_b\phi = D_a\phi D^a\phi$, are neglected in eq. (11) because they are small compared with the term linear in ϕ (see eq. (5)). On the other hand, since the spatial average of $D_aD^a\phi$ vanishes, the neglect of the spatial average of nonlinear terms like $D_a\phi D^a\phi$ in eqs. (9) and (10) is justified as follows. We have

$$\begin{aligned} \int_V D_a\phi D^a\phi dV &= - \int_V \phi D_aD^a\phi dV \\ &= -4\pi \int_V \phi \delta\rho dV \\ &= -4\pi \int_V \phi (\rho - \bar{\rho}) dV. \end{aligned}$$

The integral of $\phi\rho$ is much less than the integral of ρ , as $\phi \ll 1$ and ρ is nonnegative. The same argument holds for the $\phi\bar{\rho}$ term. Thus, under our assumptions, the spatial average of $D_a\phi D^a\phi$ is much less than $\bar{\rho}$, which justifies dropping the former in eqs. 9 and 10.

flow, which, for convenience, we take to be located at $r = 0$. To do so we define a new radial coordinate, R , by

$$R = ar, \quad (13)$$

and a new time coordinate, T , by

$$T = \tau + \frac{1}{2} \frac{\dot{a}}{a} R^2. \quad (14)$$

In these new coordinates the metric of Eq. (1) takes the form

$$ds^2 = -(1 + 2\phi - R^2\ddot{a}/a) dT^2 + \left(1 - 2\phi + R^2 \left[(\dot{a}/a)^2 + k/a^2 \right]\right) dR^2 + (1 - 2\phi)R^2 d\Omega^2, \quad (15)$$

where we have dropped all terms of order R^3 and higher in distance from the origin. Transforming to an isotropic radial coordinate, then further transforming to the corresponding Cartesian coordinates X, Y, Z , and, finally, substituting from Einstein's equations (Eqs. (9) and (10)) for the underlying Robertson-Walker model, we obtain

$$ds^2 = -(1 + 2\Phi - \Lambda R^2/3) dT^2 + (1 - 2\Phi - \Lambda R^2/6)[dX^2 + dY^2 + dZ^2], \quad (16)$$

where

$$\Phi \equiv \phi + 2\pi R^2 \bar{\rho}/3, \quad (17)$$

and where, to the approximation in which we are working (i.e., dropping terms of order R^3 and higher), we have $R^2 = X^2 + Y^2 + Z^2$. Thus, Φ satisfies the ordinary Poisson equation

$$\begin{aligned} \nabla^2 \Phi &= \nabla^2 \phi + 4\pi \bar{\rho} \\ &= 4\pi(\delta\rho + \bar{\rho}) \\ &= 4\pi\rho. \end{aligned} \quad (18)$$

When $\Lambda = 0$, Eq. (16) is precisely the usual form of Newtonianly perturbed Minkowski spacetime (see, e.g., Sec. 4.4a of [6]). Thus, in the spacetime of Eq. (1), when $\Lambda = 0$, Newtonian gravity holds to a very good approximation in the vicinity of any observer following the Hubble flow, where ‘‘in the vicinity’’ here means on scales much smaller than the Hubble radius. Even when $\Lambda \neq 0$, if $|\delta\rho| \gg \bar{\rho}$ in the neighborhood of the observer, realistic values

of Λ have $\Lambda R^2 \ll \Phi$ out to distances much smaller than the Hubble radius. Thus, Newtonian gravity holds to an excellent approximation in the vicinity of such observers as well.

In summary, we may characterize our cosmological model of Eq. (1), together with Eqs. (3)–(5), as one which corresponds closely to a Robertson-Walker model as far as the Hubble flow of the matter and the causal structure of the spacetime are concerned, but in which the local distribution of matter may be highly inhomogeneous. In addition, as we have just noted, on scales small compared with those set by the underlying Robertson-Walker model, Newtonian gravity holds to a very good approximation. Apart from negligibly small regions of spacetime which contain black holes or other strong field objects, we believe that our universe is accurately described by this model. In any case, our model is a relatively precise, mathematically consistent cosmological model which describes the spacetime structure and distribution of matter on all scales, and is not in obvious conflict with any observed properties of our universe.

1.2 Propagation of Photon Beams

Let us now consider this cosmological model from the perspective of photons (\equiv null geodesics) propagating in it, and compare this to what photons would encounter in a Robertson-Walker model. All gravitational focusing and shearing effects on an infinitesimal beam of light rays in the vicinity of a null geodesic γ are described by the geodesic deviation equation (see, e.g. [6])

$$\frac{d^2 \eta^a}{d\lambda^2} = -R_{bcd}{}^a k^b k^d \eta^c, \quad (19)$$

where k^a is the tangent to γ corresponding to affine parameter λ , and η^a is the deviation vector to an infinitesimally nearby null geodesic in the beam. The Riemann curvature tensor appearing in Eq. (19) can be decomposed into its Ricci and Weyl pieces in the usual way (see, e.g. [6])

$$R_{abcd} = C_{abcd} + (g_{a[c} R_{d]b} - g_{b[c} R_{d]a}) - \frac{1}{3} R g_{a[c} g_{d]b}. \quad (20)$$

The Ricci curvature directly produces a rate of change of convergence of the beam of geodesics, while the Weyl curvature directly produces a rate of change of shearing.

In a Robertson-Walker model the Weyl tensor vanishes and, by Einstein's equation, the Ricci tensor is of the form $R_{ab} = 8\pi(T_{ab} - 1/2 Tg_{ab})$, with T_{ab} given by Eq. (6). The geodesic deviation equation then takes the form

$$\frac{d^2\eta^a}{d\lambda^2} = -4\pi\omega^2\rho\eta^a, \quad (21)$$

where ω is the frequency of the photon as measured in the Robertson-Walker rest frame. This corresponds to a steady increase in the convergence of the beam of geodesics, with no shear. Contrast this behavior with the propagation of photons in the cosmological model of Eq. (1) in the case where the matter is highly clumped on various scales, but with no (or negligible) matter distributed between the clumps. In this case, the Ricci tensor vanishes along the geodesic, except for rare instances when the photon propagates through a clump of matter. On these rare occasions, the Ricci curvature briefly becomes extremely large compared with that of the underlying Robertson-Walker model. The Weyl curvature also will be small except in similarly rare instances of propagation through (or very near) a sufficiently dense clump of matter. Thus, when the matter distribution is highly clumped, at almost all times the propagation of a beam of photons in the spacetime of Eq. (1) would be indistinguishable from propagation in flat spacetime. Occasionally, however, the beam may receive a strong “kick” of Weyl and/or Ricci curvature. Thus, the local history of a photon propagating in the spacetime of Eq. (1) could hardly be more different from the local history of a photon propagating in a Robertson-Walker model! Nevertheless, there are some global correspondences. In particular, since the causal structure of the spacetime of Eq. (1) corresponds closely to that of the underlying Robertson-Walker metric, at each redshift⁴ the area of the boundary of the past of an event in the spacetime of Eq. (1) must be very nearly equal to the area of the past light cone of the corresponding event in the underlying Robertson-Walker metric. We will return to this point in Subsection 4.2.

In order to calculate magnification and shear effects on a (nearly) point source due to gravitational lensing, we need to integrate the geodesic deviation equation (Eq. (19)) along a null geodesic connecting the source to the observer. To do this, we need to know the curvature along the geodesic. The

⁴Since $|\phi| \ll 1$ and the velocity of matter relative to the Hubble flow is small, we neglect the difference between redshifts in the metric of Eq. (1) and in the underlying Robertson-Walker model.

curvature is determined directly by a knowledge of the underlying Robertson-Walker model together with ϕ . We will assume that, in the underlying Robertson-Walker model, the distance scales set by the spatial curvature and Λ are at least as large as the Hubble radius, R_H . The spacetime curvature of the Robertson-Walker model is then of order $1/R_H^2$. Contributions of ϕ to the spacetime curvature which are smaller than $1/R_H^2$ will therefore be neglected. From Eq. (11), together with the assumption that ϕ is bounded and has vanishing spatial average, it follows that ϕ is uniquely determined by specifying the matter distribution $\delta\rho$. However, Eq. (11) is a nonlocal equation, so in principle the locally encountered curvature could depend upon the distribution of matter in arbitrarily distant parts of the universe.⁵ Nevertheless, we shall now argue that, under our cosmological assumptions, only the distribution of matter within R_H is relevant.

1.3 The Local Nature of the Influence of Matter on Photon Beams

Let S be a sphere of proper radial distance R_H centered about the point x at which we wish to evaluate ϕ . Let $G_D(x, x')$ denote the Dirichlet Green's function for the equation $a^{-2}h^{ab}D_aD_bG(x, x') = -4\pi\delta(x, x')$ for the region enclosed by S . (A simple, explicit formula for G_D in the case of flat geometry can be found, e.g., in Sec. 2.6 of [7].) Then, by Green's identity, we have

$$\phi(x) = - \int_V G_D(x, x')\delta\rho(x')dV' - \frac{1}{4\pi} \int_S \phi(x')\hat{r}'^a D'_a G_D(x, x') dS', \quad (22)$$

where the volume integral extends only over the region enclosed by S . Under our above assumptions, the contribution of ϕ to the curvature is given directly in terms of the second spatial derivatives of ϕ , since the contributions from the time derivatives of ϕ , products of first derivatives of ϕ , etc., have been assumed to be negligible compared with the linear contributions from the second spatial derivatives of ϕ . Differentiating Eq. (22), we obtain

$$\begin{aligned} D_a D_b \phi(x) &= - \int_V D_a D_b G_D(x, x')\delta\rho(x') dV' \\ &\quad - \frac{1}{4\pi} \int_S \phi(x')\hat{r}'^a D'_a D_a D_b G_D(x, x') dS'. \end{aligned} \quad (23)$$

⁵Note that since, for an open universe, $\delta\rho$ does not fall off to zero at infinity, we cannot assume, a priori, that ϕ is given in terms of $\delta\rho$ by the usual Poisson integral expression that would hold for a localized mass distribution.

However, the surface term in Eq. (23) is of order $|\phi|/R_H^2$, and thus, in view of Eq. (3), it can be neglected. Therefore the curvature at x is determined by the matter distribution only within a Hubble radius of x , as we desired to show. It should be emphasized that this conclusion is *not* a consequence of any causality arguments but, rather, follows directly from our above *assumption* that ϕ is small at distances of order R_H , as is necessary for the underlying Robertson-Walker metric to be a good description of spacetime structure on cosmological scales.

We now make the additional assumption that there is a (co-moving) scale $\mathcal{R} \ll R_H$ such that no strong correlations in the distribution of matter occur on scales greater than \mathcal{R} . Under these circumstances it seems clear that the curvature at a given point can be accurately calculated—at least for the purposes of determining geodesic deviation—by taking into account only the matter distribution within a distance \mathcal{R} of that point. We have not attempted to give a precise formulation or proof of this claim, but a justification for it can be given as follows. First we note that, by Einstein’s equation, the Ricci curvature is determined by the matter distribution in a completely local manner. Therefore, matter can have a nonlocal influence on a photon beam only via Weyl curvature. To calculate the Weyl curvature associated with a distribution of matter we need to evaluate the trace-free part of the second derivatives of ϕ , as given by Eq. (23) with the surface term omitted. We break up the volume V in Eq. (23) into a union of regions of size \mathcal{R} , excluding the ball of radius \mathcal{R} centered at x . In the case of flat spatial geometry, each of these regions will make a contribution of order m/D^3 to the Weyl tensor at x , where D is the distance of the region from x , and m is of the order of the expected mass, $\bar{\rho}\mathcal{R}^3$, contained in that region. However, by our assumption, there will be no correlations between the contributions from the different regions. Hence, by a simple “random walk” estimate, we find that the total contribution to the Weyl tensor at x from all of V except for the ball of radius \mathcal{R} centered at x should be no greater than $\sim m/\mathcal{R}^3 \sim \bar{\rho}$. Similar estimates hold if the geometry is curved or a cosmological constant is present, since G_D will differ significantly from the flat case only at distances comparable to R_H , and the contributions from these regions should be negligible.

We note that $\bar{\rho}$ is the same order of magnitude as the curvature of the underlying Robertson-Walker metric. A Ricci curvature of this magnitude and having a consistent sign (as occurs in the Robertson-Walker model) could have a significant effect on the convergence of a beam of photons propagating over cosmological distances. However, a randomly fluctuating Weyl curvature

of this magnitude should have a completely negligible effect upon the shear (merely adding a tiny bit of “noise” to the Weyl curvature resulting from nearby matter), and an even smaller effect upon the convergence. Thus, no significant error should be made by considering only the curvature resulting from the presence of matter within \mathcal{R} of the photon path, as we desired to show.

Since we have assumed that $\mathcal{R} \ll R_H$ and that the distance scales set by the spatial curvature and/or Λ are at least as large as R_H , the Dirichlet Green’s function within \mathcal{R} of x will be well approximated by $1/r$, where r denotes the proper distance between x and x' . Thus, Eq. (22)—with the surface term omitted and the volume integral restricted to a ball of radius \mathcal{R} around x —reduces to the usual Poisson integral formula, and the curvature can be obtained from formulas arising from ordinary Newtonian gravity (see Sec. 2 below). It is somewhat more convenient to work with the potential Φ of Eq. (17) rather than ϕ . It follows that Φ is given by the usual Poisson integral formula of ρ (rather than $\delta\rho$) over the region enclosed by \mathcal{R} .

1.4 Our Method

The basic idea of our procedure in its most general context can now be explained. We choose an underlying Robertson-Walker model and (co-moving) scale, \mathcal{R} , with $\mathcal{R} \ll R_H$ in the present universe.⁶ We then specify a probability distribution for how the matter is distributed within \mathcal{R} . This probability distribution may vary with cosmological time; it is constrained only by the requirement that the average amount of mass contained within \mathcal{R} agree with that occurring in the underlying Robertson-Walker model. We then perform a “Monte Carlo” propagation of a beam of photons backward in time, starting from the present, in the following manner: We prescribe a matter distribution (chosen from our probability distribution) in a ball of radius \mathcal{R} . We calculate the Newtonian potential for this matter distribution, and the corresponding curvature. Then we choose a random impact parameter for the entry of a photon into this ball, and we integrate Eq. (19) through the ball. (In this step, we take the photon trajectory to be a “straight line”, i.e., we do not attempt to include the (completely negligible) corrections due to the tiny bending angle.) When the photon exits from this ball, we use the underlying

⁶More generally, we could specify a probability distribution for \mathcal{R} , although we shall not do so in this paper.

Robertson-Walker model to update the frequency of the photon relative to the local rest frame of the matter, and to update the proper radius corresponding to the comoving scale \mathcal{R} . Then we choose a matter distribution in a new ball of comoving radius \mathcal{R} , choose another random impact parameter for entry of the photon into this ball,⁷ and repeat the above calculations. We continue until the photon has reached the desired redshift. By repeating this sequence of calculations a large number of times—for most of our models we performed about 2,000 such “runs”—we build up good statistics on what happens to beams of photons on our past light cone. From this we obtain, for any given model, good statistical information on the magnification, shear, and rotation of images of (nearly) point sources at any redshift. We will spell out the details of our procedure more explicitly in the next section.

In comparison with other approaches, ours most closely resembles the “Swiss cheese” models, wherein one takes a matter dominated Robertson-Walker model, removes the dust from spherical balls, and redistributes the mass within these balls in some other (arbitrarily chosen) spherically symmetric manner. However, it differs from the Swiss cheese models in the following significant ways: (i) The “cheese” has been completely eliminated. (ii) The mass within a given ball need not be equal to the corresponding Robertson-Walker mass, though equality must still hold on average. (iii) The matter distribution within the balls need not be spherically symmetric. (iv) We do not consider the propagation of photons in a single, fixed cosmological model. Rather, each photon in effect “creates its own cosmological model” via our Monte Carlo procedure during the course of its propagation. (v) Although it is not a necessary facet of the Swiss cheese models, most analyses of the Swiss cheese models [8, 9] have attempted to calculate only averages of certain lensing quantities, and, in the course of doing so, have imposed an “opaque radius” cutoff—within which photons are absorbed—which biases the results towards defocusing relative to Robertson-Walker models. Our analysis determines the probability distributions for magnification, shear, and rotation of sources by doing an exact, Monte Carlo calculation, imposing no opaque radius cutoff. As we shall see, our results show no bias towards defocusing relative to the underlying Robertson-Walker model, provided that all of the high luminosity images are included (see Sec. 6 for further discussion).

Our approach also bears some similarity to analyses which start with a

⁷Note that, in general, this would require the balls to overlap slightly. We neglect this overlap in our analysis.

model of the matter distribution in the universe—obtained analytically [10, 11, 12] or from N-body codes [13, 14, 15, 16]—and then project the matter into lens planes lying between the source and observer. Ray shooting methods are used to numerically obtain bending angles of a large sample of photons, from which the amplification and shear distribution of images can then be computed. Our approach uses the geodesic deviation equation rather than the lens equation and is considerably simpler and more flexible. It also avoids any artifacts resulting from putting all the matter into lens planes.

1.5 The Relevant Scales of Clustering and Clumping

Two final issues remain to be addressed: (1) What clustering scale \mathcal{R} should be chosen to adequately model statistical lensing effects in our universe, i.e., what is the largest scale on which the clustering of matter has an important effect upon lensing? (2) On what scales (below \mathcal{R}) does one have to model the details of the matter distribution in order to adequately treat statistical lensing effects, i.e., what is the smallest scale on which the clumping of matter has an important effect?

In analyzing these questions, it is convenient to view galaxies as the basic “building blocks” of the distribution of matter in the universe. (Although we do not exclude the possibility that substantial amounts of matter may be distributed between galaxies, we assume that such matter is distributed in a relatively uniform way.) It is essential to take into account the clumping of matter on the scale of galaxies in order to adequately model lensing effects. In essence, the first question above asks to what extent the clustering of the galaxies themselves must be taken into account, while the second question asks to what extent the clumping substructure of the matter within galaxies must be taken into account.

As already noted, it follows from Einstein’s equation that the Ricci curvature is determined by the matter distribution in a completely local manner. The effects of Ricci curvature on lensing should therefore depend only upon the density contrasts associated with galaxies, and not upon the “shape” of galaxies. This will be verified explicitly in Subsection 4.2. Furthermore, these Ricci curvature effects should depend only weakly on the clustering of galaxies, since the clustering should merely produce some correlations in the times of passage of a photon through different galaxies, and these effects should largely “wash out” over cosmological distance scales. Thus, we believe that the clustering of galaxies should have a negligible influence on lensing

effects produced by Ricci curvature.

On the other hand, simple estimates show that the Weyl curvature of a spherical aggregate of matter of mass m and radius r can have a substantial effect on lensing only if the matter “lies within its own Einstein radius”, r_E , i.e., only if

$$r^2 \lesssim r_E^2 \sim mD, \quad (24)$$

where D denotes a cosmological distance and we use units where $G = c = 1$. Note that this relationship is marginally satisfied by individual galaxies (or at least by their central cores), so the Weyl curvature of individual galaxies can (at least occasionally) produce significant lensing effects. Clustering of galaxies can produce important Weyl curvature effects only in circumstances when the clusters themselves satisfy Eq. (24). This *does* occur in the central portions of rich clusters of galaxies, so the effects of clustering cannot always be assumed to be negligible.

However, in the limit where galaxies can be treated as “point masses”—as occurs if Eq. (24) is satisfied by a wide margin—it follows from the analysis given in Subsection 3.2 below that even very strong clustering of the galaxies will have at most a tiny effect on the lensing probability distributions for the magnification, shear, and rotation of (nearly) point sources. (On the other hand, clustering *would* still have an important effect on some lensing quantities, such as bending angles, which we do not calculate here.) Thus, clustering effects can be of importance for the statistical lensing quantities treated here only when individual galaxies fail to satisfy Eq. (24), but these galaxies form clusters which satisfy Eq. (24) (at least in their core regions). In these circumstances the neglect of the clustering of galaxies should underestimate the lensing effects somewhat. However, we do not believe that such circumstances arise frequently enough to have an important influence on the statistical lensing quantities we calculate. Furthermore, as we shall conjecture in Subsection 3.4, the point mass results should provide a firm upper limit to lensing effects, even when galactic clustering is present.

Consequently, in this paper we shall take \mathcal{R} to be the scale of the separation between galaxies, thereby neglecting lensing effects resulting from the clustering of galaxies. For the reasons detailed above, we do not expect that this will result in any significant errors in our calculations of the probability distributions for magnification, shear, and rotation of images of cosmologically distant sources. Some evidence in favor of this expectation will be given in Section 6, where we will obtain results in close agreement with [15],

despite our neglect of the effects of clustering.⁸

We turn now to the issue of how small a scale of clumping of matter we must consider in order to calculate gravitational lensing effects. In principle the clumping of matter on arbitrarily small scales (including atomic and sub-atomic scales) could have an important effect on lensing—though we would have to use physical, rather than geometric, optics to calculate these effects when the objects are so small that the scale of variation of the gravitational field becomes less than the wavelength of the light. However, the finite size of the source which is being lensed provides an effective cutoff to lensing produced by clumping on small scales. This follows because the lens merely magnifies (as well as shears and rotates) the image of the source, keeping the surface brightness constant [11]. Thus, if the angular size of the (assumed to be uniform) source is much larger than the angular scale associated with the lens, the lensing effects caused by clumping should have little effect, as only a relatively small part of the source would be magnified by the presence of a clump of matter (and the rest of the source may be correspondingly demagnified by the absence of matter between clumps). In other words, the net angular size of the image of a source of finite size will not be significantly affected by sufficiently small scale lensing, and consequently, the luminosity of the image also will not be greatly affected.⁹ The angular scale of the source is $\sim r_S/D_S$, where r_S denotes the size of the source and D_S denotes its distance, and the angular scale associated with the lens is $\sim r_E/D_L$, where D_L denotes the distance of the lens. Taking D_S and D_L to be cosmological in scale and using Eq. (24) for r_E , we find that lensing effects should not be important unless the mass of the lens satisfies

$$m \gtrsim r_S^2/D. \quad (25)$$

The smallest sources of interest here (central regions of quasars and supernova shells at an early stage of expansion) have $r_S \gtrsim 10^{-3}$ light years, so taking $D \sim 10^{10}$ light years, we find

$$m \gtrsim 10^{-3}M_\odot. \quad (26)$$

⁸This expectation could be further tested by re-doing our analysis taking \mathcal{R} to be the scale of separation of clusters of galaxies and using appropriately chosen probability distributions for the distribution of mass within clusters. We have not yet attempted to carry out such an analysis.

⁹If the angular size of the source is much larger than the angular scale of separation between the clumps of matter, then the lensing effects of the matter should wash out completely.

Clumping of matter on mass scales smaller than Eq. (26) should not be relevant for the sources we consider. However, the clumping of matter down to the scale of Eq. (26) is potentially of importance. In particular, the clumping of matter in galaxies into stars can have a significant effect upon the probability distribution for the magnification of light emitted from quasars and supernovae.

Fortunately, it is not necessary to model a galaxy as 10^{11} or so point mass stars in order to calculate its lensing effects. The clumpiness of matter will be relevant only very close to the path of the photon. If, say, we let $d \sim 100r_E$, where r_E denotes the Einstein radius of a single star, then the discreteness of the galactic mass distribution due to stars which lie outside of a tube of radius d around the photon path can be ignored, i.e., outside of the tube the galactic matter distribution can be treated as continuous. Consequently, in our analysis we will take account of all “microlensing” effects due to small scale clumping of matter (say, into stars) in the following manner: First, we model the galaxy as a continuous mass distribution and compute its Newtonian potential. Then, when a photon passes through the galaxy in our Monte Carlo simulations, we remove the continuous galactic matter lying within cylindrical radius d of the path (or the portion of this matter assumed to be clumped into stars), and subtract the Newtonian potential of this removed matter. Finally, we randomly redistribute this removed mass back into the cylinder in the form of stars, and we add in the Newtonian potential of these “point masses”. In this manner we take full account of the small scale clumping of matter in a computationally efficient way.

2 Details of Our Method

In the previous section we spelled out our cosmological assumptions and described our method for calculating statistical lensing effects on cosmological sources. The purpose of this section is to provide a more concrete and explicit description of our approach.

As discussed in the previous section, we first must choose an underlying matter dominated Robertson-Walker model, which we may characterize by the parameters (H_0, Ω_0, Λ) , where the subscript “0” denotes the present value, and where $\Omega_0 \equiv 8\pi\bar{\rho}_0/3H_0$. (The value of k can then be determined from Einstein’s equation (10).) For the calculations in this paper, we use the value $H_0 = 70 \text{ km s}^{-1} \text{ Mpc}^{-1}$. We choose a comoving scale, \mathcal{R} , which, as

discussed above, we take to be the scale of the galactic separations. For most of the calculations in this paper the value of \mathcal{R} will be taken to correspond to 2 Mpc in the present universe. Next we specify how mass is distributed in (and in between) galaxies. As explained in the previous section, in general, we may specify this as a probability distribution which is subject only to the constraint that, on average, the mass assigned to the galaxy equals the mass contained in a ball of radius \mathcal{R} in the underlying Robertson-Walker model. In the present paper, however, we will only be concerned with simple “toy models” for the mass distribution, and, in each model universe, we will take all galaxies to have identical mass and structure, rather than specifying a probability distribution. (However, we will consider model universes with a wide range of different galactic mass distributions.) We also will choose the galactic mass distributions (expressed in terms of proper—not comoving—distances) not to vary with cosmological time.

Our basic strategy for determining lensing effects can be explained in the following manner. Imagine a telescope at an event p in the present universe which is pointed in some direction in the sky, so that it only accepts photons which impinge upon it with null tangent very close to the direction k^a . Suppose, further, that k^a has been chosen so that, when followed backwards in time, a photon arriving at event p with null tangent k^a would have emerged from a source at redshift z , i.e., suppose that the telescope happens to be “pointed at” a source at redshift z . If the source is sufficiently small, the photons emitted by it which are accepted by the telescope can be treated as a beam of null geodesics which all lie on the past light cone of p and have directions differing only infinitesimally from k^a . The deviation vector characterizing any given geodesic in this beam must therefore vanish at p , and is uniquely determined by its time derivative at p . The relationship between the image produced by the telescope and the actual structure of the source is determined by the relationship between the time derivatives of the deviation vectors in this infinitesimal beam at p and the values of these deviation vectors at redshift z . To calculate this relationship we must integrate the geodesic deviation equation (19)—*backwards* in time starting from p —for the 2-dimensional space of spatial deviation vectors η^a which are orthogonal to k^a and which vanish at p . By linearity of the geodesic deviation equation, the components of these deviation vectors in a parallelly propagated frame are determined by a 2×2 matrix, $\mathcal{A}^\mu{}_\nu(\lambda)$, defined by

$$\eta^\mu(\lambda) = \mathcal{A}^\mu{}_\nu(\lambda) \frac{d\eta^\nu}{d\lambda}(0), \quad (27)$$

where $\lambda = 0$ corresponds to the present time. It follows immediately from the geodesic deviation equation (19) that $\mathcal{A}^\mu{}_\nu(\lambda)$ satisfies

$$\frac{d^2 \mathcal{A}^\mu{}_\nu}{d\lambda^2} = -R_{\alpha\beta\sigma}{}^\nu k^\alpha k^\sigma \mathcal{A}^\beta{}_\mu, \quad (28)$$

with initial conditions $\mathcal{A}^\mu{}_\nu(0) = 0$ and $d\mathcal{A}^\mu{}_\nu(0)/d\lambda = \delta^\mu{}_\nu$. Equation (28), together with these initial conditions, uniquely determines $\mathcal{A}^\mu{}_\nu$ for all λ .

All lensing effects considered in this paper are obtained directly from $\mathcal{A}^\mu{}_\nu$ as follows. Let λ_z denote the affine parameter of the beam of photons at redshift z . We decompose the matrix $\mathcal{A}^\mu{}_\nu(\lambda_z)$ as a product of a proper (i.e., unit determinant) orthogonal matrix $O^\mu{}_\nu$ and a self-adjoint matrix $S^\mu{}_\nu$

$$\mathcal{A}^\mu{}_\nu(\lambda_z) = O^\mu{}_\sigma S^\sigma{}_\nu. \quad (29)$$

The matrix S can be characterized by its two eigenvalues, α_1 and α_2 . The area, A , of the beam at redshift z is given by

$$A = \alpha_1 \alpha_2 = \det \mathcal{A}. \quad (30)$$

The corresponding magnification—and, hence, amplification—of the (nearly point) source at redshift z (relative to a source placed at the same affine parameter in flat spacetime) is given by

$$\mu = \lambda_z^2 / A. \quad (31)$$

Note that a caustic in the beam of geodesics occurs precisely when $\det \mathcal{A} = 0$, in which case the magnification/amplification of a point source becomes infinite.

The distortion of the image is characterized by the ratio, ϵ , of the eigenvalues of \mathcal{A}

$$\epsilon = |\alpha_1 / \alpha_2|, \quad (32)$$

where we take $|\alpha_1| \leq |\alpha_2|$, so that $0 \leq \epsilon \leq 1$. For a circular source, the image will be elliptical in shape, with axial ratio given by ϵ . This distortion also can be characterized by the net shear¹⁰ of the image, defined by

$$\gamma = \frac{|\alpha_1 - \alpha_2|}{2\lambda_z}. \quad (33)$$

¹⁰The term “shear” is also commonly used for the optical tensor σ_{ab} (see, e.g., (9.2.28) of [6]) and/or its magnitude, σ . These quantities characterize the “rate of shearing” of the beam, and should be clearly distinguished from the “net shear” defined here.

If $A > 0$, corresponding to a beam which has not passed through a caustic (or has passed through an even number of caustics), we may choose S to be positive definite (as opposed to negative definite). This uniquely fixes O . The matrix O can be characterized, in turn, by a rotation angle Θ ranging between $-\pi$ and π , which may be interpreted as the angle of rotation of the image relative to the orientation that the image would have had in the underlying Robertson-Walker model. Such a rotation results from the cumulative effects of shearing in different directions produced by masses lying in different “lens planes”; lensing by masses lying in a single plane orthogonal to the photon trajectory would not yield any rotation. If $A < 0$, there is a sign ambiguity in S , and a corresponding sign ambiguity in O . We resolve this ambiguity (arbitrarily) by choosing Θ to range between $-\pi/2$ and $\pi/2$.

In this paper, the desired statistical information on the magnification, shear, and rotation of sources at redshift z will be obtained by repeated “Monte Carlo” integration of Eq. (28), as explained in detail below. It is worth noting that Eq. (28) corresponds to the “primitive form”, (Eq. (19)), of the geodesic deviation equation, rather than the mathematically equivalent “optical equations” form (see, e.g., Eqs. (9.2.32)–(9.2.33) of [6]) used in many other analyses. For our purposes, Eq. (28) has a significant advantage over the optical equations in that \mathcal{A}^μ_ν varies continuously when caustics occur, whereas quantities—such as the convergence of the congruence—appearing in the optical equations become singular at caustics.

We begin our backwards evolution of Eq. (28), with initial conditions $\mathcal{A}^\mu_\nu(0) = 0$ and $d\mathcal{A}^\mu_\nu(0)/d\lambda = \delta^\mu_\nu$, by imagining that the beam of photons enters a ball of radius \mathcal{R} with a randomly chosen impact parameter, b , i.e., we take $b = \sqrt{p}\mathcal{R}$ with p chosen randomly from the interval $[0, 1]$. As described above, the mass distribution in this ball has been prescribed, and we can calculate the Newtonian potential, Φ , corresponding to this mass distribution by solving the ordinary Poisson equation (see Eq. (18) above). The relevant components of the Riemann curvature tensor can be calculated straightforwardly for the metric of Eq. (16), yielding

$$\begin{aligned} R_{abcd}k^bk^d &= 2\omega^2\partial_a\partial_c\Phi + k^b\partial_b(k^d\partial_d\Phi)\eta_{ac} \\ &= \omega^2[2\partial_a\partial_c\Phi + Z^b\partial_b(Z^d\partial_d\Phi)\eta_{ac}]. \end{aligned} \quad (34)$$

Here η_{ab} denotes the ordinary Minkowski metric associated with the coordinates (T, X, Y, Z) (see Eq. (16) above), ∂_a denotes the derivative operator of η_{ab} , Z^a denotes a unit vector in the “ Z -direction” (\equiv the direction of

propagation of the photon), and $\omega = dT/d\lambda$ denotes the frequency of the photon. Without loss of generality, we choose our affine parametrization so that initially $\omega = 1$. Note that the Λ term in Eq. (16) does not contribute to the relevant components of the Riemann tensor, i.e., we have *not* assumed in this equation that $\Lambda = 0$.

In integrating Eq. (28) through the ball, we neglect the tiny bending angle of the photon trajectory, and we also neglect the tiny changes in $\mathcal{A}^\mu{}_\nu$ occurring as the photon traverses the ball. Thus, when the beam of photons exits from the ball, the new values of $\mathcal{A}^\mu{}_\nu$ and $d\mathcal{A}^\mu{}_\nu(0)/d\lambda$ are related to the values they had when entering the ball as follows:

$$(\mathcal{A}^\mu{}_\nu)_1 = (\mathcal{A}^\mu{}_\nu)_0 + \omega^{-1} \Delta Z (d\mathcal{A}^\mu{}_\nu/d\lambda)_0 \quad (35)$$

$$(d\mathcal{A}^\mu{}_\nu/d\lambda)_1 = (d\mathcal{A}^\mu{}_\nu/d\lambda)_0 - \omega J^\mu{}_\beta (\mathcal{A}^\beta{}_\nu)_0, \quad (36)$$

where we have used the fact that $dZ/d\lambda = \omega$, and where we have defined

$$J^\mu{}_\nu \equiv \int dZ [2\partial^\mu \partial_\nu \Phi + Z^b \partial_b (Z^d \partial_d \Phi) \delta^\mu{}_\nu], \quad (37)$$

with the integral taken over the “straight line” photon path through the ball. Since $(\mathcal{A}^\beta{}_\nu)_0 = 0$, the $J^\mu{}_\nu$ term will not contribute to Eq. (36) for the traversal through the first ball, but it will contribute for all subsequent balls.

For the cases considered in this paper, $J^\mu{}_\nu$ can be calculated analytically. Specifically, if we align our axes so that the photon propagates in the Z -direction and lies in the $Y = 0$ plane, then for a “point mass” of mass M placed at the center of the ball (i.e., linearized Schwarzschild geometry), we have

$$\begin{aligned} (J^P)^X{}_X &= -2M \left(1 - \frac{b^2}{R^2}\right)^{1/2} \left(\frac{2}{b^2} + \frac{1}{R^2}\right) \\ (J^P)^Y{}_Y &= +2M \left(1 - \frac{b^2}{R^2}\right)^{1/2} \left(\frac{2}{b^2} + \frac{1}{R^2}\right) \\ (J^P)^X{}_Y &= 0, \end{aligned} \quad (38)$$

where b is the impact parameter and R is the proper radius of the ball ($= \mathcal{R}$ for the initial ball). For a uniform density ball of mass M and radius d concentric with the ball of radius R , we have for $b \leq d$,

$$(J^U)^X{}_X = (J^P)^X{}_X + 4M \left(1 - \frac{b^2}{d^2}\right)^{1/2} \left(\frac{1}{b^2} + \frac{2}{d^2}\right)$$

$$\begin{aligned}
(J^U)^Y_Y &= (J^P)^Y_Y - 4M \left(1 - \frac{b^2}{d^2}\right)^{1/2} \left(\frac{1}{b^2} - \frac{1}{d^2}\right) \\
(J^U)^X_Y &= 0,
\end{aligned} \tag{39}$$

whereas $(J^U)^\mu_\nu = (J^P)^\mu_\nu$ when $b > d$. Similarly, for a truncated isothermal ball (with density given by $\rho \propto 1/r^2$) of mass M and ‘‘cutoff radius’’ d , we have for $b \leq d$,

$$\begin{aligned}
(J^I)^X_X &= (J^P)^X_X + \frac{4M}{b^2} \left(1 - \frac{b^2}{d^2}\right)^{1/2} \\
(J^I)^Y_Y &= (J^P)^Y_Y - \frac{4M}{b^2} \left(1 - \frac{b^2}{d^2}\right)^{1/2} + \frac{4M}{bd} \cos^{-1}(b/d) \\
(J^I)^X_Y &= 0,
\end{aligned} \tag{40}$$

and, again, the point mass expressions apply when $b > d$. Finally, for a uniform density cylinder of cylindrical radius d and length $2R$, whose axis passes through the center of the ball of radius R , when the photon trajectory does not pass through the cylinder, we have

$$\begin{aligned}
(J^C)^X_X &= -\frac{2(1 + \cos^2 \alpha)\gamma}{\sin \alpha} \left[\frac{Z_+}{X_0^2 + Z_+^2} - \frac{Z_-}{X_0^2 + Z_-^2} \right] \\
(J^C)^Y_Y &= +\frac{2(1 + \cos^2 \alpha)\gamma}{\sin \alpha} \left[\frac{Z_+}{x_0^2 + Z_+^2} - \frac{Z_-}{X_0^2 + Z_-^2} \right] \\
(J^C)^X_Y &= 4\gamma X_0 \cot \alpha \left[\frac{1}{X_0^2 + Z_+^2} - \frac{1}{X_0^2 + Z_-^2} \right],
\end{aligned} \tag{41}$$

where we have neglected the tiny ‘‘end effects’’ resulting from the finite length of the cylinder. In Eq. (41), the axes have been aligned so that the photon again propagates in the Z -direction, but now the X and Y axes are chosen so that the shortest line connecting the photon path to the axis of the cylinder points in the X -direction. The length of this shortest line is X_0 , whereas α denotes the angle between the path of the photon and the axis of the cylinder. The quantities Z_- and Z_+ denote, respectively, the Z -values of the entry and exit of the photon from the ball of radius R , with $Z = 0$ being the point of closest approach of the photon path to the axis of the cylinder. Finally, $\gamma \equiv M/2R$ denotes the mass per unit length of the cylinder. When the photon trajectory passes through the cylinder, the additional

term $16\gamma(d^2 - X_0^2)^{1/2}/(d^2 \sin \alpha)$ must be added to $(J^C)^X_X$, but the other components of $(J^C)^\mu_\nu$ are not changed.

The x and y axes of our parallelly propagated frame will be rotated by an angle θ with respect to the X and Y axes of the above formulas. Under a rotation, U , by angle θ , components of J transform as

$$J \rightarrow UJU^{-1} \quad (42)$$

so that, explicitly, the components of J in our parallelly propagated frame are given by

$$J^x_x = \cos^2 \theta J^X_X + \sin^2 \theta J^Y_Y - 2 \sin \theta \cos \theta J^X_Y, \quad (43)$$

and so on.

We return, now, to following the evolution (into the past) of our beam of photons. After the beam exits from the first ball, it is assumed to immediately enter a second ball. However, on account of the Hubble expansion—or, rather, the Hubble contraction, since we are evolving backwards in time—the proper radius, R , of the second ball will now be smaller than \mathcal{R} by the factor a_1/a_0 , where a_0 and a_1 denote, respectively, the values of the scale factor of the underlying Robertson-Walker metric at the times of entry into, and exit from, the first ball. Similarly, the frequency of the photons will be blueshifted by this same factor. After updating the values of R and ω in this manner, we send the beam of photons into the second ball with a randomly chosen impact parameter, and with a randomly chosen value of the orientation angle, θ , with respect to the parallelly propagated frame (see Eq. (43)). (In the cylindrical case, the orientation of the axis of the cylinder also is suitably randomized.) When it exits the second ball, the values of \mathcal{A}^μ_ν and $d\mathcal{A}^\mu_\nu/d\lambda$ are changed via Eqs. (35) and (36). The values of R and ω are then also updated, and the beam of photons is subsequently taken to enter a third ball. This procedure is repeated until the desired redshift is reached. At each redshift the area, shear, and rotation of the beam can be computed in the manner explained below Eq. (29).

Fig. 1 shows the area of a beam of geodesics as a function of z for a typical “run”, in the case of a universe with $\Omega = 1$ and $\Lambda = 0$, and where the galaxies are treated as point masses. The corresponding areas for the underlying Robertson-Walker model and for a universe which is empty near the beam (i.e, $R_{abcd} = 0$ in a neighborhood of the beam) are also shown (see [17]). In this particular run, it can be seen that the beam of photons

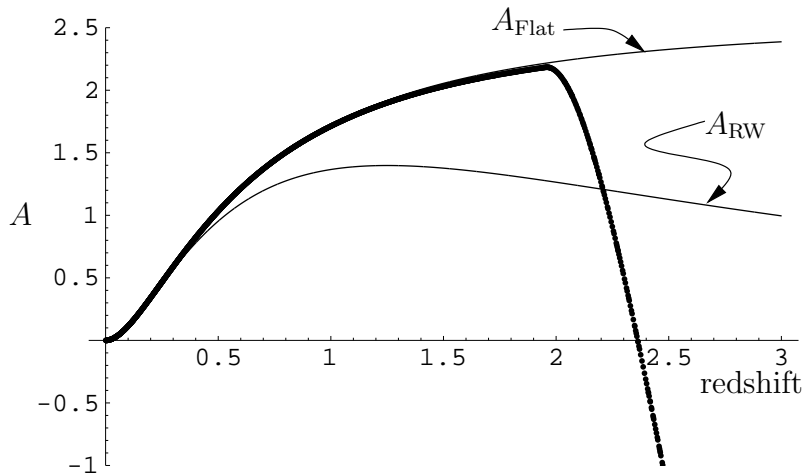


Figure 1: The area vs. redshift of a beam of photons in a typical Monte-Carlo run, for a universe with $\Omega_0 = 1$ and $\Lambda = 0$ in which all of the matter is in the form of point masses.

propagates very nearly as though it were in empty, flat spacetime, until it reaches a redshift $z \simeq 2$, at which time it receives a strong “kick” due to a close encounter with a (point mass) galaxy. A caustic then occurs at a redshift $z \simeq 2.4$. To build up good statistics, we typically performed 2,000 such “runs” for each choice of cosmological model (i.e., values of Ω_0 and Λ) and galactic mass distribution. Our results will be presented in the following sections.

Finally, we explain in more detail how the effects due to clumping of matter into stars (or other sub-galactic structures) are calculated. First, a continuous mass distribution is specified for the galaxy, and the $J^\mu{}_\nu$ appropriate to this continuous distribution was obtained (see Eqs. (38)–(41) above). A cylindrical radius d is then chosen so that a typical cylindrical tube cutting through the galaxy contains at least ~ 10 “stars”. For the cases we consider, such a d is automatically much smaller than galactic scales, but much larger than the Einstein radius of the individual stars. In our “runs”, when a beam of photons passes through a galaxy, we replace the $J^\mu{}_\nu$ calculated for the continuous mass distribution by $J'^\mu{}_\nu$ where

$$J'^\mu{}_\nu = J^\mu{}_\nu - 4\pi\sigma \delta^\mu{}_\nu + \sum_i (J_i^P)^\mu{}_\nu(b_i, \theta_i). \quad (44)$$

Here σ is the projected surface density (mass per unit area) of the galaxy at the photon trajectory, m_s denotes the mass of an individual star, the “impact parameters” b_i are chosen randomly within a disk of radius d , and the rotation angles θ_i are chosen randomly in $[0, 2\pi]$. The sum ranges up to $N \approx m/m_s$, where $m = \pi d^2 \sigma$ is the mass in a cylindrical tube of radius d about the photon path. The term $-4\pi\sigma \delta^\mu_\nu$ subtracts the contribution to J^μ_ν from the continuously distributed mass within the cylindrical tube, whereas the last term corresponds to adding back in the contribution of this mass in the form of (point mass) stars, where each J_i^P is given by Eq. (38) as modified by Eq. (43). (As we shall see in the next section, no essential change in the probability distribution for J^μ_ν would occur if we put the entire mass m into a single “star” which is randomly distributed in the disk of radius d .) We believe that all statistical “microlensing” effects due to stars or other sub-galactic structures can be accurately taken into account by this procedure.

3 Point Masses and Spherical Clustering

In this section we will analyze lensing effects in the limiting case where all of the matter in the universe is clumped into structures which are much smaller than their own Einstein radii, so that these objects may be treated as point masses. By a combination of analytic and numerical arguments, we will establish—or, at least, present strong evidence for—the following two key claims: (1) If the point masses are randomly distributed throughout the universe, then the probability distributions for magnification, shear, and rotation of images depend, in an essential way, only on the total mass density of the point masses. (This mass density, of course, is constrained to equal the mass density of the underlying Robertson-Walker model.) In other words, these probability distributions are (virtually) independent of the masses of the individual point masses; in particular, they are (virtually) the same for a universe randomly populated by stellar mass black holes (or stars) as for a universe randomly populated by galactic mass black holes. (Some partial results along this line are given on P. 329 of [11].) (2) If the point masses are not randomly distributed but are clustered on scales $\ll R_H$ in a spherical but otherwise arbitrary manner, then the probability distributions for magnification, shear, and rotation of images are very nearly the same as for the randomly distributed case.

Taken together, results (1) and (2) provide a great strengthening of the familiar claim that the “optical depth” for a strong gravitational lensing event produced by point masses depends only on the total mass density of these point masses [18]. We show here that for a universe populated by point masses, the entire probability distributions for magnification, shear, and rotation at each redshift do not depend in an essential way on either the individual masses or clustering properties of the point masses. Thus, the point mass probability distributions for magnification, shear, and rotation are remarkably “universal” in character, depending only upon the choice of underlying Robertson-Walker model. Our computations of this universal probability distribution for various choices of Ω_0 and Λ will be given in Subsection 3.3.

It should be emphasized that various lensing effects with null geodesics which differ by a *finite* (as opposed to infinitesimal) amount *will* depend on the masses and clustering properties of the individual point masses. In particular, if the lensing of a given source produces multiple images, the expected angular separation of these images will depend strongly on the masses and/or clustering properties of the point masses. What we show here, however, is that for a universe populated by point masses, all of the statistical properties of the *individual images* of nearly point sources are “universal”—although the criteria for what constitutes a “nearly point source” does depend upon the properties of the point masses (see Eq. (25) above).

3.1 Random Distributions of Point Masses

We turn now to a demonstration of claim (1). As in the previous section, consider the propagation of a beam of photons backwards in time. We focus attention on the lensing effects caused by matter near the photon trajectory at redshift z . We may view this matter as lying in a single “lens plane”. Suppose a point mass of mass M is randomly placed in this lens plane within a disk of radius L centered on the photon trajectory. By Eqs. (35) and (36), the effect of this mass on \mathcal{A}^μ_ν is determined by J^μ_ν . Setting $R \rightarrow \infty$ in Eq. (38), and performing the rotation indicated in Eq. (43), we obtain

$$\begin{aligned} J^x_x &= -\frac{4M \cos 2\theta}{b^2} \\ J^y_y &= \frac{4M \cos 2\theta}{b^2} \end{aligned} \tag{45}$$

$$J_y^x = -\frac{4M \sin 2\theta}{b^2},$$

where (b, θ) (with $b \in [0, L]$) denote the polar coordinates of the point mass. It follows that the lensing effects of the point mass on the beam of photons are uniquely determined via Eq. (45) by a knowledge of the probability distribution, $p(\psi)$, for the variable

$$\psi \equiv \frac{4M \cos 2\theta}{b^2}, \quad (46)$$

corresponding to a random choice of point in the disk. A straightforward calculation yields

$$p(\psi) = \frac{4M}{\pi L^2 \psi^2} \begin{cases} 1 - \sqrt{1 - (L^4 \psi^2 / 16M^2)} & \text{if } L^4 \psi^2 / 16M^2 < 1 \\ 1 & \text{otherwise} \end{cases} . \quad (47)$$

Note that this probability distribution has a divergent second moment (and the integral defining the first moment fails to converge absolutely).

Now suppose we break up the point mass, M , into N point masses, each of mass $m = M/N$. Suppose we randomly distribute these N point masses within the same disk of radius L in the given lens plane. The corresponding J^μ_ν produced by this configuration of masses is given by a formula similar to Eq. (45), except that M is replaced by M/N and a sum is taken over the independent contributions of the N particles. By inspection, we see that the probability distribution for J^μ_ν in this case is determined by the probability distribution, $P_N(\Psi)$, for the variable Ψ in exactly the same manner as the probability distribution for J^μ_ν in the case of a single mass is determined by $p(\psi)$, where

$$\Psi \equiv \frac{1}{N} \sum_{i=1}^N \psi_i, \quad (48)$$

and where each ψ_i is given by Eq. (46) with (b, θ) taken to be the polar coordinates of the i th particle. Thus, the lensing effects of a single, randomly distributed point mass of mass M will differ from the lensing effects of N randomly distributed point masses, each of mass M/N , precisely to the extent that the probability distribution functions p and P_N differ.

The determination of the relationship between p and P_N is a standard problem in probability theory: If p is the probability distribution for the random variable ψ , then $P_N(\Psi)$ corresponds to the probability that the average

value of a series of N independent “trials” will be Ψ . If p is such that its second moment is finite, the answer to this problem in the limit of large N is known as the “law of large numbers”, which states that P_N is well approximated by a Gaussian centered at $\langle\psi\rangle$ whose width is proportional to $1/\sqrt{N}$. However, the law of large numbers is *not* applicable here because, as already noted above, the probability distribution of Eq. (47) fails to have a finite second moment. We note in passing that the failure of p to have a finite second moment implies that if one wishes to work with moments of p , it will be necessary to impose an “opaque radius” cutoff to the probability distribution at large ψ , as has been done in most analyses of the “Swiss cheese” models. No opaque radius cutoff will be imposed here.

Although the law of large numbers does not hold here, the mathematical techniques used in the proof of the law of large numbers can be used to analyze the relationship between p and P_N (see [11]). We write

$$P_N(\Psi) = \int \delta\left(\Psi - \frac{1}{N}\sum_{i=1}^N \psi_i\right) p(\psi_1) \cdots p(\psi_N) d\psi_1 \cdots d\psi_N. \quad (49)$$

Taking the Fourier transform of P_N , we obtain

$$\begin{aligned} \hat{P}_N(K) &\equiv \int e^{-iK\Psi} P_N(\Psi) d\Psi \\ &= \int e^{-iK\psi_1/N} \cdots e^{-iK\psi_N/N} p(\psi_1) \cdots p(\psi_N) d\psi_1 \cdots d\psi_N \\ &= [\hat{p}(K/N)]^N, \end{aligned} \quad (50)$$

where \hat{p} is the Fourier transform of p . A direct computation of \hat{p} from Eq. (47) yields

$$\hat{p}(k) = 1 - 4M|k|/L^2 + O(k^2). \quad (51)$$

In the limit as $N \rightarrow \infty$, we have

$$\begin{aligned} \hat{P}_\infty(K) &= \lim_{N \rightarrow \infty} \left(1 - \frac{4M|K|}{NL^2}\right)^N \\ &= \exp(-4M|K|/L^2). \end{aligned} \quad (52)$$

Taking the inverse Fourier transform of Eq. (52), we obtain

$$P_\infty(\Psi) = \frac{4M}{\pi L^2} \frac{1}{\Psi^2 + \alpha^2}, \quad (53)$$

where $\alpha \equiv 4M/L^2$.

A number of key conclusions follow directly from Eq. (53). First, the mere existence of P_∞ is somewhat surprising, since, *a priori*, there is no obvious reason to expect a well defined, finite, and nonvanishing limit to the lensing effects of randomly distributed point masses as $N \rightarrow \infty$. More remarkable still is the fact that P_∞ nearly coincides with the original probability distribution p ; they are both “ $1/x^2$ ” distributions with the same coefficient, but are “regularized” in slightly different ways near $x = 0$. Furthermore, the small difference between $P_\infty(x)$ and $p(x)$ at $x \approx 0$ is of no importance because the contribution to lensing is negligible in that regime. Thus, the probability distributions for magnification, shear, and rotation of images for the case where a single point mass is randomly placed in a lens plane will differ negligibly from the limiting case where infinitely many infinitesimal point masses (with the same total mass) are randomly placed in that lens plane.

The fact that P_∞ is an excellent approximation to p further implies that for finite N , P_N also can differ only negligibly from p . Indeed, if we approximate p by P_∞ in Eq. (50), we find $P_N \approx P_\infty$, i.e., to the extent that we have $p \approx P_\infty$ we also have $p \approx P_N$ for all N . Consequently, an arbitrary (finite) subdivision of a point mass placed randomly in a given lens plane has essentially no effect on the statistical distributions of lensing images, provided, of course, that all of the point masses resulting from this subdivision are again randomly distributed. Since an arbitrary spectrum of masses can be produced by appropriate subdivisions starting from a single point mass, this result has the further consequence that the random placement of *any* collection of point masses of total mass M in a given lens plane has the same effect on the statistical distributions of the lensing images as a single point mass of mass M . Finally, since the cumulative lensing effects produced by all of the matter in the universe can be viewed as resulting from a sequence of encounters of the beam of photons with matter lying in various different lens planes, we conclude that *all* random distributions of point masses throughout the universe (of *any* mass spectrum) must produce the same statistical distributions of the lensing images, as stated in claim (1) above.

As a check of both the above arguments and our methods for calculating lensing effects, we have tested claim (1) in the following ways: First, we computed the statistical distributions of the lensing images for a universe with $\Omega = 1$ and $\Lambda = 0$ by the method of Section 2, taking the “galaxies” to be point masses of mass $M = 10^{12}M_\odot$. This should correspond closely to

the case of a universe filled with a random distribution of point masses, each having mass $10^{12}M_{\odot}$. Then we repeated the Monte Carlo calculations choosing $M = 10^{13}M_{\odot}$, and taking \mathcal{R} to be correspondingly larger. The results we obtained for the two cases were statistically indistinguishable from each other. We also repeated our calculations with “galaxies” taken to be uniform density balls of radius $d = \mathcal{R}$ (so that the matter is distributed exactly as in the underlying Robertson-Walker model), but taking “microlensing” by “stars” into account in the manner explained at the end of Section 2. This calculation corresponds to a universe filled with a random distribution of point masses each of mass $M = M_{\odot}$. Again, the results we obtained were statistically indistinguishable from the two previous cases.

3.2 Spherical Clustering of Point Masses

The results of the previous subsection apply only to random distributions of point masses. What happens if the point masses are clustered? On one hand, since clustering produces corresponding “voids”, there should be an increased likelihood that the photon beam will fail to come close to any point mass. Furthermore, if the photon beam passes near to some point mass, there is an increased likelihood that the lensing effects of this point mass will be partially canceled by the presence of other nearby point masses. These two effects suggest that clustering should decrease the overall lensing efficiency of point masses. On the other hand, clustering will result in the production of a large scale, coherent “cluster potential”, which can cause important lensing effects on the beam of photons even if this beam does not pass close to any individual point mass. This effect suggests that clustering should increase the overall lensing efficiency of point masses.

In fact, our results for randomly distributed point masses strongly suggest that the above effects should nearly cancel, at least for spherical clustering. Imagine starting with a random distribution of point masses, each of mass M . Suppose we cluster N of these point masses into a spherical structure of radius d . This clustering should have little effect upon lensing unless d is sufficiently small that the Einstein radii of the individual masses overlap when projected into the plane perpendicular to the path of the photon [19]. However, at this stage, d will be of the order of the Einstein radius of the cluster. If d is made still smaller, the cluster itself can be treated as a “point mass”, and, by claim (1), its lensing effects will be equivalent to that of the original unclustered distribution. Thus, except perhaps for a cluster whose

size is very nearly equal to its own Einstein radius, spherical clustering of point masses should have a negligible effect on the statistical distributions of the lensing images, in accord with claim (2).

We have tested the above arguments for claim (2) by performing a number of runs for both uniform density and isothermal galaxies of various radii, using the “microlensing” procedure described at the end of Section 2. These calculations simulate the clustering effects of “point mass stars” into galaxies. We found that the statistical distributions of the lensing images were indeed statistically indistinguishable from the randomly distributed point mass case except when the radius of the galaxy was close to its own Einstein radius. In that case, the clustering produced a slight—but statistically significant—diminution of the lensing effects as compared with a random distribution of point masses. However, even when we chose the parameters of the galaxy so as to maximize the differences, the effects of clustering were not significant, as will be illustrated in Fig. 10 below. Thus, to an excellent approximation, for a universe with matter in the form of point masses, the statistical distributions for the magnification, shear, and rotation of images is universal in character, independent of the mass distribution and (spherical) clustering properties of the point masses.

3.3 Results

We now present some of the results of our Monte Carlo calculations of these distributions for several cosmological models. As already indicated at the beginning of Section 2, in our calculations we used the values $H_0 = 70$ km/s Mpc and $\mathcal{R} = 2$ Mpc, with the mass, M , of each galaxy then determined from the underlying Robertson-Walker model. Thus, for a universe with $\Omega = 1$, we set $M = 5 \times 10^{12} M_\odot$, whereas for a universe with $\Omega_0 = 0.1$, we set $M = 5 \times 10^{11} M_\odot$. We then performed the calculations described in detail in Section 2, using Eq. (38) for J^μ_ν . In each case presented here, we performed 2,000 “runs” back to a redshift of 3, and we calculated the magnification, shear, and rotation of the beam of photons at various intermediate redshifts as well.

The main focus of our attention was on the distribution of magnifications, since that distribution is most relevant to the applications described in Sections 5 and 6 below. We plot our magnification results in the following manner: At the given redshift of interest, our data set contains 2,000 individual values of area—one for each “run”. We sort these runs in order of

increasing value of area, with the area of beams which have passed through a caustic counting as negative (i.e., the large negative areas come first).¹¹ We then normalize the areas to the area of the underlying Robertson-Walker model, so that an image corresponding to a beam with $A = 1$ has exactly the same apparent luminosity it would have had in that model. In other words, images of objects carried by beams of photons with $|A| < 1$ have been magnified/amplified with respect to Robertson-Walker, while those with $|A| > 1$ have been demagnified/deamplified.

In our figures we plot the area of each run against its position in the sorted list. For convenience, we re-scale the x -axis so that it ranges up to 100 rather than 2,000. Thus, for a given area value A , the corresponding x -value yields the percentage of beams with area less than A . This “percentage” is taken relative to a random sampling of telescope directions in the present sky, as opposed to a random sampling of source positions at redshift z . Note that if a source is randomly placed on a sphere of radius D centered on us (with D chosen so that the light reaching us was emitted at redshift z), the probability that it will be “hit” by a given photon beam is proportional to the magnitude of the area, $|A|$, that the beam has at redshift z . A large beam will sample a larger section of the sky, and therefore will represent more sources (all of them demagnified) than a small beam. The probability that a randomly placed source will have an image with area between A and $A + \Delta A$ is proportional to the corresponding value of $\Delta x \times |A|$, rather than just Δx . We will discuss this further in Section 6 below (see Eq. (55)).

Note also that since lensing simply magnifies or demagnifies images relative to the underlying Robertson-Walker model—but does not affect the surface brightness of the images—the apparent luminosity of an image of a source is proportional to $1/A$. Since, as just noted above, the probability that a beam “hits” a given source is proportional to A , the expected luminosity (i.e., photon flux) in each beam is exactly the same as in the underlying Robertson-Walker model. In particular, our analysis automatically builds in the fact that the expected total luminosity agrees with that of the underlying Robertson-Walker model.

For beams of photons which have not undergone caustics, the largest possible area is the “flat space” (or “empty beam” [17]) value, A_{Flat} , corre-

¹¹In some cases, a handful of runs contained beams which had passed through two caustics (and thus had (usually very large) positive area). When such double-caustic runs occurred, we sorted them so that their areas appeared first, i.e., before any of the negative areas arising from single caustic runs.

sponding to setting the curvature to zero in the geodesic deviation equation. This value is marked on (most of) the figures. It should be noted that after a photon beam undergoes a caustic, its area typically becomes very large (and negative)—significantly larger in magnitude than the flat space value. (An indication of this fact can already be seen in Fig. 1.) To avoid problems with the scale of our figures, we did not attempt to plot any area values less than $-A_{\text{Flat}}$. This accounts for the “gap” at the beginning of our plots.

We will refer to an image associated with a photon beam which has not undergone a caustic as a *primary image*.¹² If p denotes the event representing our telescope at the present time, then any event q which lies on the boundary of the past of p must be connected to p by a null geodesic whose corresponding photon beam has not undergone a caustic (see, e.g., [6]). Since the world line of any source must intersect the boundary of the past of p , it follows that every source must have at least one primary image (see also [11]). In Subsection 4.2 below we shall argue that for spherical distributions of matter it is very rare that a source would have more than one primary image, but for very dense cylindrical matter distributions, multiple primary images are common. Every primary image of a source must be at least as bright as it would be if it were placed in flat spacetime at the same affine parameter distance [11]. On the other hand, secondary images (corresponding to photon beams which have undergone one or more caustics) can be arbitrarily faint. Of course, a secondary image of a source can also be bright and, in particular, can be brighter than a primary image of that source.

Each secondary image of a source must have at least one associated primary image of the same source, and (since the total number of images must be odd [11]) must also have other associated secondary images. If the angular separation of these images is very small, it may not be possible to resolve the separate images. One of the shortcomings of our method is that we do not have a good way of determining (even statistically) which primary and secondary images are associated with each other, since this would require us to analyze photon trajectories which differ by finite (as opposed to infinitesimal) separations. Thus, if the different images of the same source are not resolved—the case of microlensing—we are unable to predict the probability distribution in total luminosity.

Figs. 2–5 show our results for a universe filled with point masses corresponding to an underlying spatially flat Robertson-Walker cosmology with

¹²This corresponds to the “type I” image of [11].

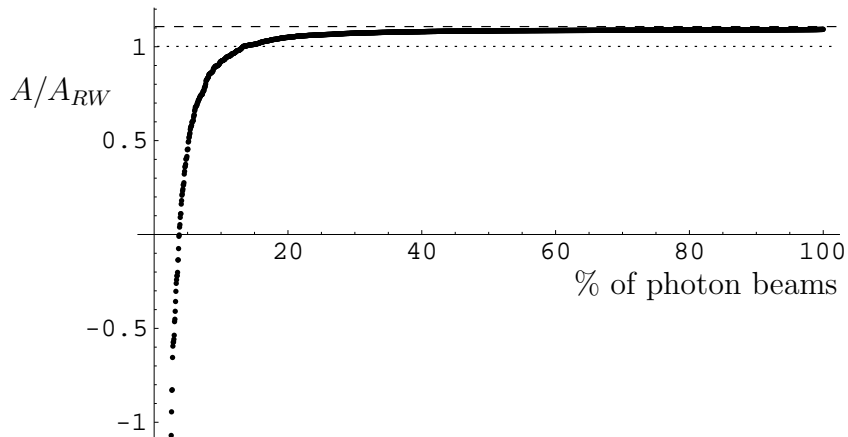


Figure 2: Area vs. % of photon beams at $z = 0.5$, for an $\Omega = 1$, $\Lambda = 0$ universe, with matter distributed in the form of point masses. The dashed line represents the flat spacetime (empty beam) area, and the dotted line represents the Robertson-Walker area.

$\Omega = 1$ and $\Lambda = 0$. As with all plots shown here, we have taken $H_0 = 70 \text{ km s}^{-1} \text{ Mpc}^{-1}$. We also took $\mathcal{R} = 2 \text{ Mpc}$, although as argued above, the results should be independent of the choice of \mathcal{R} . As can be seen from the graphs, the percentage of photon beams which have undergone caustics ranges from about 5% at redshift $z = 1/2$ to over 35% at redshift $z = 3$. Note also that by redshift $z = 3$ about 20% of the primary images are less than half as bright ($A > 2$) as they would have been in the underlying Robertson-Walker cosmology. Taking account of the factor of $|A|$ mentioned above, and assuming that each source has only one primary image (see Subsec. 4.2 below), we find that the probability that the primary image of a randomly placed source at $z = 3$ will be demagnified relative to Robertson-Walker by at least a factor of 2 is $1/2$. Since these photon trajectories do not pass near any of the point masses, it seems unlikely that such sources will have any (bright) secondary images. Thus, even if multiple images cannot be resolved, it appears that in this cosmology, at redshift $z = 3$, 50% of all sources should be dimmer by at least a factor of 2 relative to the underlying Robertson-Walker model.

The results at $z = 3$ for a universe filled with point masses corresponding to an open Robertson-Walker model with $\Omega_0 = 0.1$ and $\Lambda = 0$ is plotted in

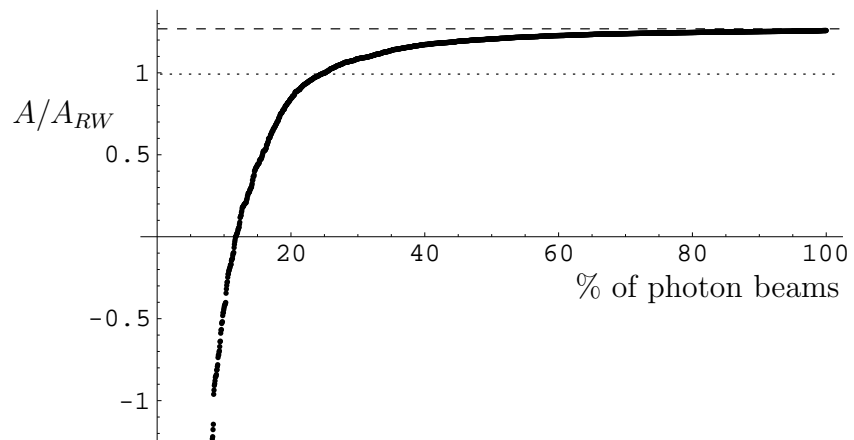


Figure 3: Area vs. % of photon beams at $z = 1.0$, for an $\Omega = 1$, $\Lambda = 0$ universe. Matter is distributed in the form of point masses.

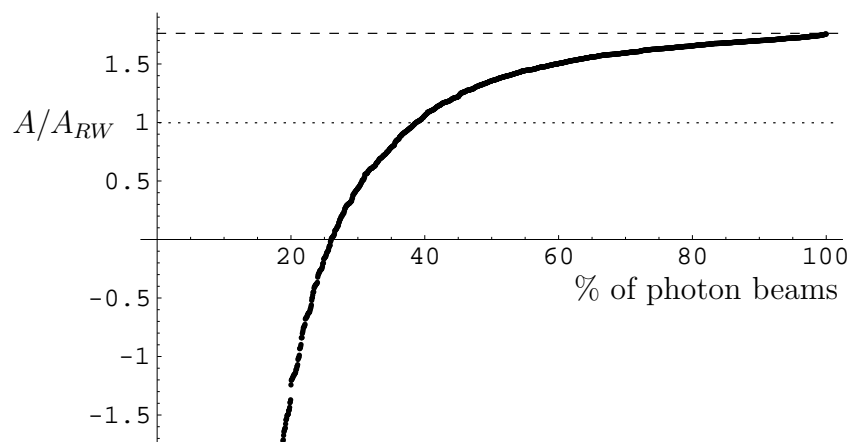


Figure 4: Area vs. % of photon beams at $z = 2.0$, for an $\Omega = 1$, $\Lambda = 0$ universe. Matter is distributed in the form of point masses.

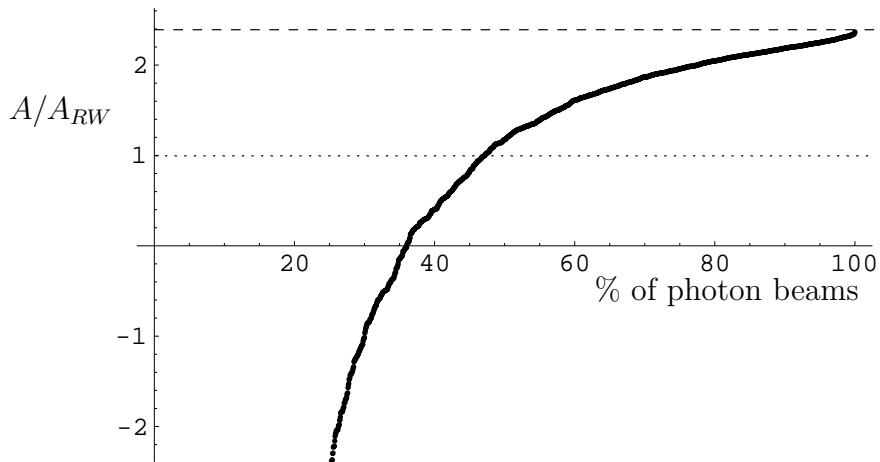


Figure 5: Area vs. % of photon beams at $z = 3.0$, for an $\Omega = 1$, $\Lambda = 0$ universe. Matter is distributed in the form of point masses.

Fig. 6. It can be seen that the lensing effects here are dramatically weaker than in the $\Omega = 1$ model. In particular, in this cosmology less than 10% of the photon beams have undergone a caustic by $z = 3$, and the maximum de-magnification relative to Robertson-Walker is only 0.85 (but over half the primary images suffer nearly this de-magnification).

Finally, the results at $z = 3$ for a universe filled with point masses corresponding to a spatially flat Robertson-Walker model with $\Omega_0 = 0.1$ and $\Omega_\Lambda \equiv \Lambda/3H_0^2 = 0.9$ are plotted in Fig. 7. This distribution is intermediate between the cases of $\Omega = 1$, $\Lambda = 0$ and $\Omega_0 = 0.1$, $\Lambda = 0$.

A sample of our results for shear is given in Fig. 8. Here we have plotted the magnification, μ , relative to the empty beam value, versus the axial ratio, ϵ , of the beam at redshift $z = 2$ for a universe filled with point masses for the case $\Omega = 1$ and $\Lambda = 0$. This figure corresponds to Fig. 11.12 of [11], except that we also have included the points with $\mu < 1$, arising from beams which have undergone caustics. The agreement between the figures appears to be excellent.

A sample of our results for rotation is given in Fig. 9. Here we plot the magnitude of rotation angle, $|\Theta|$ (in radians), versus photon beam number (ordered by area, as described above) at redshift $z = 3$ for a universe filled with point masses for the case $\Omega = 1$ and $\Lambda = 0$. From the figure it can

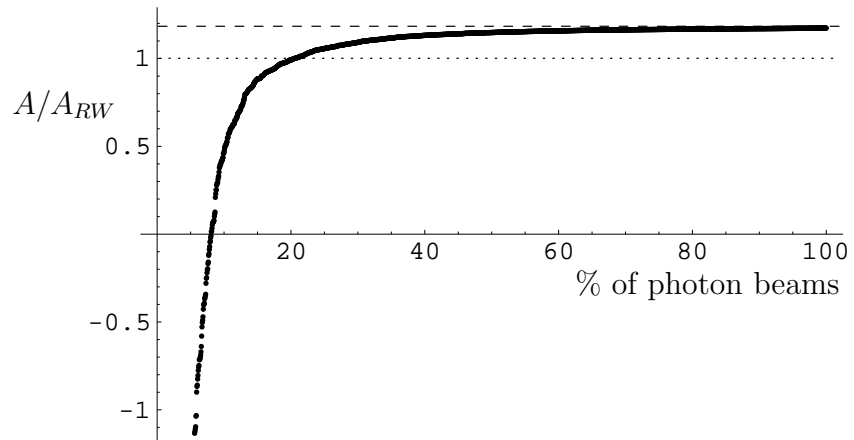


Figure 6: Area vs. % of photon beams at $z = 3.0$, for an $\Omega_0 = 0.1$, $\Lambda = 0$ universe. Matter is distributed in the form of point masses.

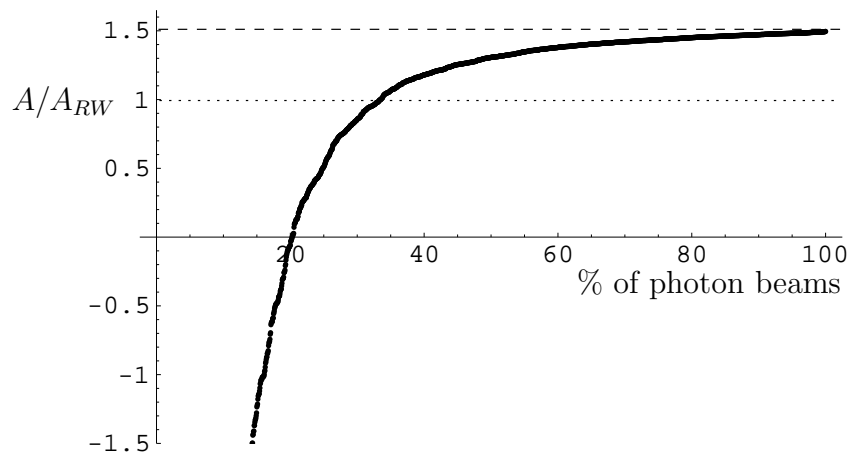


Figure 7: Area vs. % of photon beams at $z = 3.0$, for an $\Omega_0 = 0.1$, $\Omega_\Lambda = 0.9$ universe. Matter is distributed in the form of point masses.

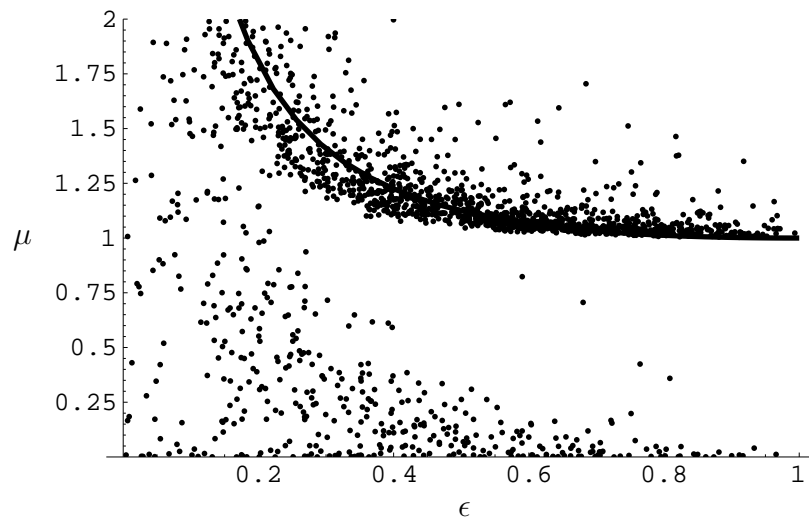


Figure 8: Magnification vs. axial ratio at $z = 2$, for an $\Omega = 1$, $\Lambda = 0$ universe filled with point masses. The solid line gives the fit $\mu = (1 + \epsilon)^2 / (4\epsilon)$, which would hold if the lensing was done by a single point mass, as described in [11]. This figure compares well with Fig. 11.12 of that reference.

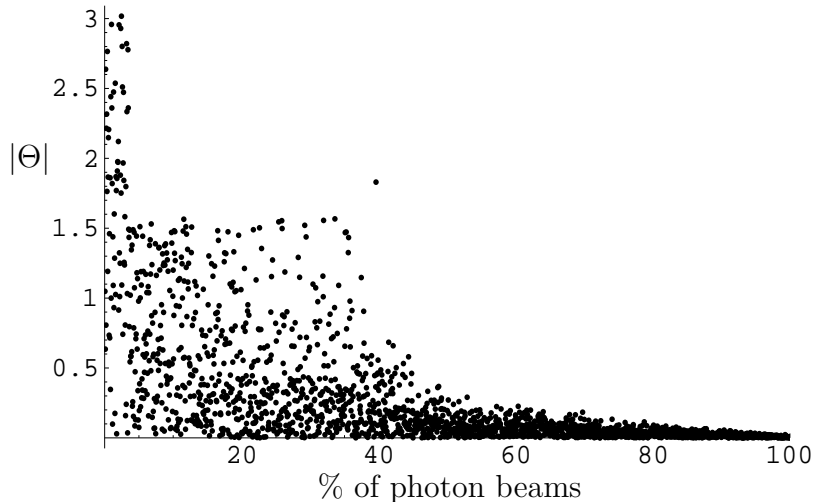


Figure 9: Magnitude of rotation angle vs. % of photon beams at redshift $z = 3$, for an $\Omega = 1$, $\Lambda = 0$ universe filled with point masses. The demarcation between beams which have undergone caustics and those which have not occurs at 36% (see Fig. 5). The restriction of $|\Theta|$ to the range 0 to $\pi/2$ (rather than 0 to π) for beams which have undergone a single caustic is due to our convention in the definition of Θ in that case, as explained below Eq. (33). The first 3% of the photon beams have undergone two caustics.

be seen that the photon beams which have not undergone caustics generally have a very small rotation, but those which have undergone caustics have undergone such a large rotation that their orientation is practically random (see [20] for a general discussion of the behavior of beams near caustics). As noted above, no rotation would occur for lensing produced by a single point mass.

Finally Fig. 10 shows how remarkably small the effects of clustering are. The right-most curve shows the magnification versus photon beam number for point mass galaxies in a universe with $\Omega = 1$ and $\Lambda = 0$, at a redshift of 3; it is the same curve as shown in Fig. 5 above. Also shown is the curve for (point mass) stars clustered into uniform density galaxies of radius 200 kpc. This curve is statistically indistinguishable from the curve for point mass galaxies. The left-most curve is for (point mass) stars clustered into uniform density galaxies of radius 20 kpc. This clustering distribution was

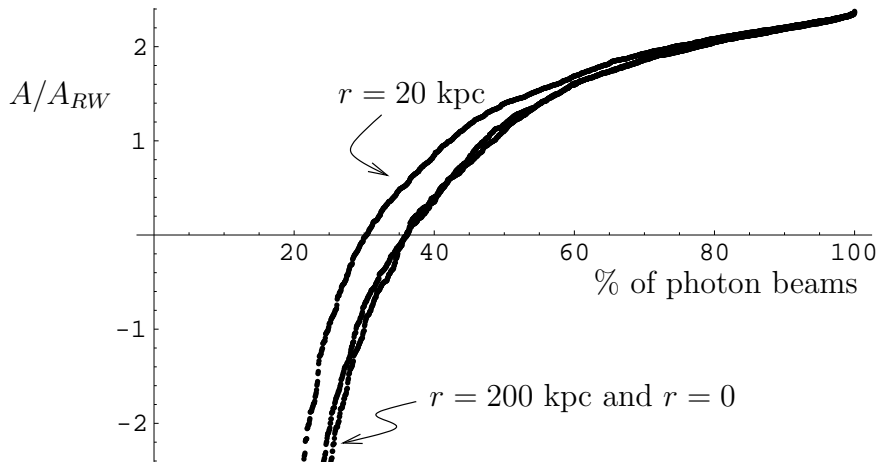


Figure 10: Area vs. % of photon beams at $z = 3$, for an $\Omega = 1$, $\Lambda = 0$ universe. Graphs are shown for point mass galaxies ($r = 0$), and for uniform density spheres of $r = 20$ kpc and $r = 200$ kpc, each composed of (point mass) stars.

chosen (in a parameter search, varying the galactic radius) so as to *maximize* the deviation from the random distribution. As expected, the maximum deviation occurs for galaxies (composed of point mass stars) whose radii are close to their Einstein radii. It can be seen from the figure that there is a slight (but statistically significant) diminution of the lensing effectiveness due to the clustering.

3.4 A Conjecture

We conclude this section with a conjecture, based upon the fact that spherical clustering of point masses appears to slightly reduce their lensing effectiveness, together with our expectation (borne out in all of our simulations) that point masses are more effective in lensing than any bodies of finite extent:

Conjecture: For any underlying Robertson-Walker cosmological model at any redshift z , randomly distributed point masses provide the most “effective” distribution of matter for lensing in the following sense: Let $A_{\text{rpm}}(x)$ denote the area as a function of the percentage of photon beams for a universe filled with a random distribution of point masses (see Figs. 2–7). Let x_1 denote the x -value such that A_{rpm} equals the Robertson-Walker

area, i.e., $A_{\text{rpm}}(x_1) = 1$. Then for any other matter distribution, we have $A(x) > A_{\text{rpm}}(x)$ for all $x \leq x_1$. In particular, the greatest number of caustics is achieved for the case of randomly distributed point masses.

4 Other Cases; Consistency Checks

4.1 Uniform Density Balls, Isothermal Balls, and Uniform Density Cylinders

In the previous section the lensing effects occurring in a universe filled with point masses were analyzed in detail. In this subsection the corresponding lensing effects will be briefly discussed for other galactic mass distributions, specifically for isothermal balls, uniform density balls, and uniform density cylinders. The isothermal balls should be good descriptions of the actual mass distribution in galaxies, so (with appropriate choices of parameters) the results for this case should provide a realistic description of the statistical lensing effects occurring in our universe—at least provided that the clustering of galaxies does not play an important role and that the effects of sub-galactic structure can be ignored. (As previously discussed near Eq. (26) above, sub-galactic structure need not be taken into account if the sources are of sufficiently large angular size. If the sources are of sufficiently small angular size that “microlensing” by stars is of relevance, and if most of the matter is in the form of stars or other condensed objects, then the point mass results of the previous section should apply.) Although the uniform density balls and cylinders presumably do not correspond to realistic mass distributions,¹³ they provide useful “toy models” for investigating various effects.

As in the point mass case, for the calculations of this subsection we used the values $H_0 = 70 \text{ km s}^{-1} \text{ Mpc}^{-1}$ and $\mathcal{R} = 2 \text{ Mpc}$, and we determined the mass, M , of each galaxy from the underlying Robertson-Walker model. Indeed, the only important difference in our calculational procedures from those of the point mass case was our use of Eqs. (39), (40), or (41) in place of Eq. (38). In addition, in the cylindrical case, a further randomization over the orientation of the cylinder was performed at each step. A sampling of

¹³Recent findings of Meiksin *et al.* [21] and others indicate that filamentary structures may play an important role in the evolution of structure. Cylindrical mass distributions can be used to mimic filaments, and identify qualitative differences in the lensing distributions to be expected from such structures.

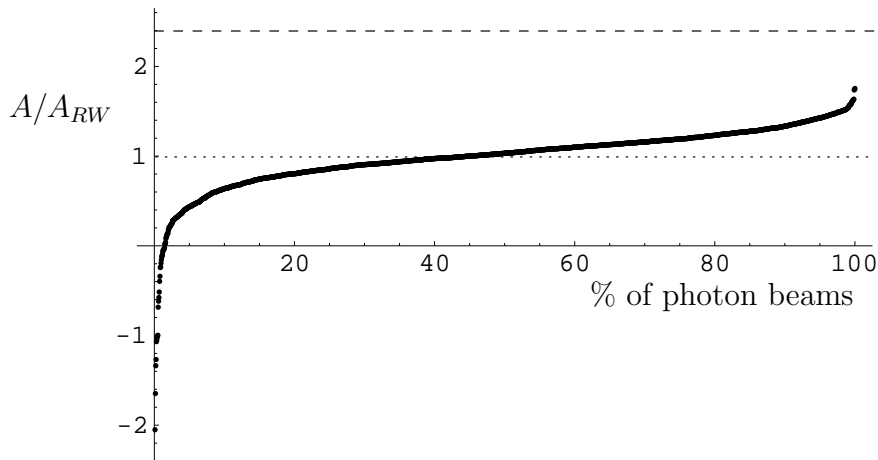


Figure 11: Area vs. % of photon beams at $z = 3.0$, for an $\Omega = 1$, $\Lambda = 0$ universe. Matter is distributed in isothermal ($M \propto r$) balls of radius 200 kpc.

some of our results is presented in Figs. 11-15.

In Fig. 11 we plot the area vs. % of photon beams at $z = 3$ for a universe with $\Omega = 1$ and $\Lambda = 0$, populated by galaxies with a “truncated isothermal profile” ($M(r) \propto r$) and a cutoff radius of 200 kpc. Comparison with Fig. 5 immediately shows that the lensing effects are greatly reduced as compared with the point mass case. In particular, only about 2% of the photon beams have undergone caustics by a redshift of 3, as compared with over 35% in the point mass case. The lensing effectiveness is further reduced if the galaxies are modeled as uniform density—rather than isothermal—balls of radius 200 kpc (see Fig. 12).

Fig. 13 shows the area vs. % of photon beams at $z = 3$ for the case $\Omega_0 = 0.1$ and $\Lambda = 0$, with matter distributed in isothermal balls, now of radius of 50 kpc. Again, a significant reduction in the lensing effectiveness as compared with the point mass case can be seen (see Fig. 6).

Finally, Figs. 14 and 15 plot the area vs. % of photon beams at $z = 3$ for the case $\Omega = 1$ and $\Lambda = 0$, with matter distributed in the form of uniform density cylinders of length $2\mathcal{R}$ and cylindrical radii 52 kpc and 200 pc, respectively. As will be discussed further below, the results shown in Fig. 15 are qualitatively different from all of the other cases shown here.

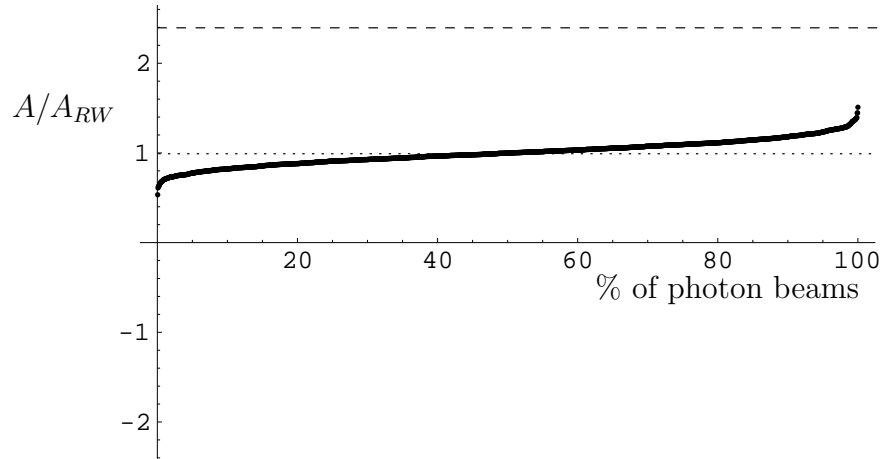


Figure 12: Area vs. % of photon beams at $z = 3.0$, for an $\Omega = 1$, $\Lambda = 0$ universe. Matter is distributed in uniform density balls of radius 200 kpc.

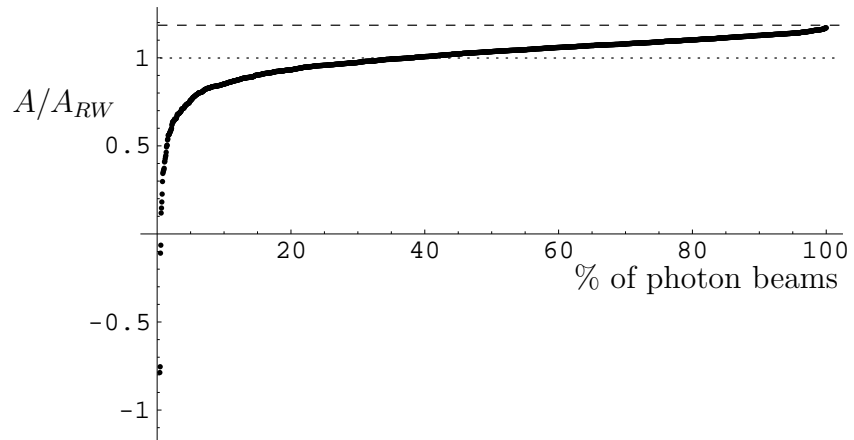


Figure 13: Area vs. % of photon beams, at $z = 3.0$, for an $\Omega_0 = 0.1$, $\Lambda = 0$ universe. Matter is distributed in isothermal balls of radius 50 kpc.

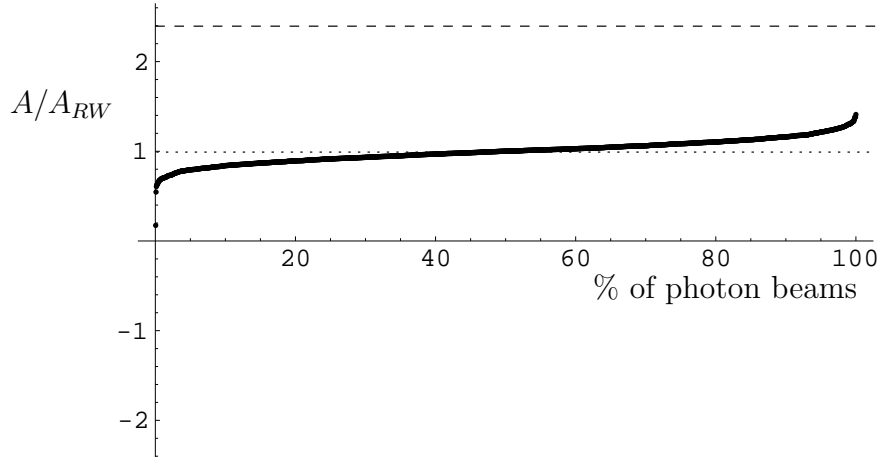


Figure 14: Area vs. % of photon beams at $z = 3.0$, for an $\Omega = 1$, $\Lambda = 0$ universe. Matter is distributed in uniform density cylinders of radius 52 kpc. This figure is almost identical to Fig. 12, which is for uniform density spheres of the same density as these cylinders.

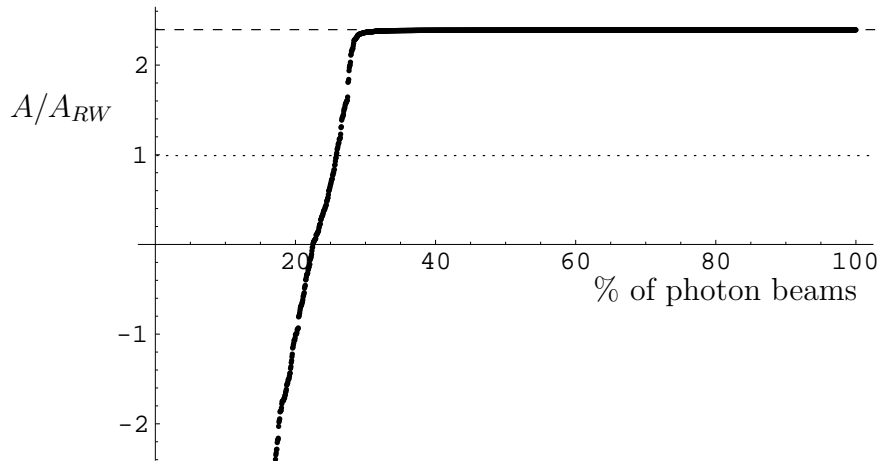


Figure 15: Area vs. % of photon beams at $z = 3.0$, for an $\Omega = 1$, $\Lambda = 0$ universe. Matter is distributed in uniform density cylinders of radius 200 pc.

4.2 Consistency Checks

The results presented thus far allow us to perform a number of consistency checks, which provide a good test of some of the underlying ideas of Section 1 as well as a good test of the validity and accuracy of our formulas and calculational procedures.

First, as noted in Subsection 1.5, the effects of Ricci curvature on lensing should depend only upon the density contrasts present in the universe. Thus, in situations where the Weyl curvature can be neglected, galaxies of the same density should produce identical statistical lensing effects, independent of their “shapes”. This is borne out by a comparison of Figs. 12 and 14, corresponding, respectively, to spherical and cylindrical galaxies of the same density. No statistically significant difference is discernible for the area distributions in these two cases.

A further important consistency check arises from the fact that the causal structure of the spacetime of Eq. (1)—whose properties we are attempting to model with our Monte Carlo calculations—is nearly the same as that of the underlying Robertson-Walker model. Consequently, at any redshift z , the area of the boundary of the past of an event p in the spacetime of Eq. (1) should be very nearly equal to the area of the past light cone of p at redshift z in the underlying Robertson-Walker model. Now, as previously mentioned in Subsection 3.3, for a null geodesic to lie on the boundary of the past of p , it is necessary that its corresponding photon beam not have undergone a caustic. Thus, in any of our Monte Carlo results, if we add up the areas of all of the photon beams which have not undergone caustics (corresponding to “primary images” in the terminology introduced in Subsec. 3.3), the result should be at least as large as the area of the past light cone in the underlying Robertson-Walker model. Since we have normalized our beam areas so that $A = 1$ corresponds to the Robertson-Walker value, this means that if we do N Monte-Carlo runs, then, within statistics, we always must have

$$\sum_i A_i \geq N, \tag{54}$$

where the sum ranges only over the beams which have not undergone caustics by the given redshift.¹⁴

¹⁴There is an additional “area test” that should hold: If we add up *all* areas—with beams with an odd number of caustics counting as negative and beams with an even number of caustics (or no caustics) counting as positive—we should (very nearly) obtain

We have checked Eq. (54) in all of our Monte Carlo simulations (including many not shown here) and have found it to be satisfied in all cases. Furthermore, in all of our simulations in which the matter distribution within \mathcal{R} is spherically symmetric (i.e., in all but the cylindrical cases), the left side of Eq. (54) was larger than the right side by only a tiny amount—typically, just a few percent. This remarkable (near) equality of the left and right sides of Eq. (54) has two important consequences. First, it provides strong evidence of the self-consistency of our calculations, since it is hard to imagine how such (near) equality could hold for cases as different as, say, Figs. 5 and 12, if our Monte Carlo calculations were not properly modeling at least some aspects of the spacetime of Eq. (1). Second, it shows that for spherical matter distributions, almost all photons which leave the boundary of the past of p do so at (or very near to) a caustic. Consequently, it also shows that in the spherical case, very few sources can have more than one primary image.

For the case of a relatively “thick” cylinder (with negligible Weyl curvature) as in Fig. 14, near equality also holds in Eq. (54), as is evident from the fact that Fig. 14 is indistinguishable from Fig. 12. However, for a very thin cylinder as in Fig. 15, the left side of Eq. (54) exceeds the right side by a factor of about 1.8. Thus, in this case many sources must have multiple primary images, presumably resulting from the passage of photons around different sides of the cylinder.

5 Correlations Between Quasar Luminosity and the Number of Absorption Systems

In a recent paper, Vanden Berk *et al.* [1] have presented evidence for a positive correlation between quasar luminosity and the number of intervening Carbon IV absorption clouds. Using the results of previous quasar surveys, these authors compiled a catalog of nearly 500 quasars, with over 2,000 heavy metal absorption lines. Analysis of this catalog revealed an excess of C IV absorbers in luminous QSOs. The authors proposed that this effect might be caused by the brightening (i.e., magnification) of the quasar images due

the Robertson-Walker result. However, it was not possible to meaningfully apply this test to our Monte Carlo data, because the total area in our data set was usually dominated by a single area value from a run which had undergone a caustic (or a double-caustic). In other words, our “statistics” were never adequate to investigate this test.

to cumulative gravitational lensing by the mass distribution associated with the C IV absorbers.

Figs. 1 and 4 of [1] present the main evidence in favor of this positive correlation. In their Fig. 1, they divide the quasars in their catalog into a “bright half” and a “dim half”, and they plot the number of C IV absorbers for the two groups in five different redshift bins. In all five bins, the bright quasars had more C IV absorbers than the dim ones. We have analyzed these results and we estimate that if the effect found in their Fig. 1 were due entirely to lensing, each C IV absorber would have to contribute an increase on the order of $1/2$ V magnitude to the luminosity of the quasar. Possible evidence for an even larger effect can be found in Fig. 4 of [1]. That figure shows a three magnitude difference between the absolute luminosity of the quasars with the largest and fewest number of C IV absorbers. Taken at face value, this suggests that each absorber would have to contribute an increase of roughly 1 V magnitude to the luminosity of the quasar for the effect to be due to lensing.

A proper analysis of the results of [1] and their implications for lensing would, of course, require a careful consideration of numerous observational issues. We shall not attempt to undertake such an analysis here.¹⁵ Nevertheless, we shall pose the following questions: Should gravitational lensing produce a systematic, positive correlation between quasar luminosity and the number of intervening absorption clouds? If so, is this effect large enough to plausibly account for the results of [1]?

To analyze these questions, we make the extreme assumption that (most of) the mass of the universe is associated with C IV absorption clouds. Clearly, this assumption should maximize the lensing effects associated with the C IV absorbers, and the results we obtain should thereby be viewed as upper limits to the possible lensing effects of these clouds. In our investigations, we considered underlying Robertson-Walker models with $\Lambda = 0$ and with Ω_0 either 1 or 0.1. For each Robertson-Walker model, we considered a variety of different possible mass distributions associated with the C IV absorbers. These mass distributions ranged from “point masses” (appropriate if the C IV clouds are associated with large black holes or with galaxies in which most of the matter has already condensed to form stars) to low density isothermal balls (corresponding to galaxies or proto-galaxies). For each cos-

¹⁵The bias due to gravitational lensing on the luminosity function of quasars has been investigated by Pei [22].

mological model and mass distribution, a “cloud radius” was defined so that in the Monte Carlo data we generated, our average number of C IV absorbers in the relevant redshift range was equal (at least approximately) to the average number of C IV absorbers in the data of [1]. We then performed the Monte Carlo calculations described in detail in the previous sections above, but in addition, we now kept track of the number of times the photon beam “passed through a C IV cloud” (i.e., had an impact parameter smaller than the assigned “cloud radius”). At each redshift of interest, we again ordered our 2,000 “runs” by area, and then binned these ordered runs in 100 groups of 20 runs each. For each such group of 20, we then computed (from our magnification data) the average magnitude of a “standard candle” source at the given redshift, as well as the average number of “passages through C IV clouds”. We then represented each of our 100 groups as a point in a “scatter plot” of average magnitude versus average number of passages through a C IV cloud.

Fig. 16 shows the results we obtained for (standard candle) quasars at a redshift of 2 for the case of a universe with $\Omega_0 = 0.1$ and $\Lambda = 0$, and with matter in isothermal balls of mass $5 \times 10^{11} M_\odot$ and radius 50 kpc. In this case, the “cloud radius” also was taken to be 50 kpc, so that each time a photon beam punctures a galaxy, we say that we have registered an absorption line. It can be seen from the figure that there is a clear positive correlation between luminosity and the number of “passages through clouds”. However, the effect is not very large, corresponding to only about 0.1 magnitude per absorber.

The results we obtained in a variety of other cases were quite similar. In all the cases we examined, a positive correlation was found between quasar luminosity and the number of “passages through clouds”. When we made the mass distribution associated with the clouds more highly concentrated than in Fig. 16, the lensing effect on luminosity became larger, but the correlation with the number of clouds generally became less strong (since the lensing effects were more dominated by a single close encounter), so the overall results were not greatly changed. Thus, none of the cases we investigated produced lensing effects which deviated significantly from the roughly 0.1 magnitude per absorber seen in Fig. 16. This value is undoubtedly an overestimate since, as mentioned above, in our calculations we associated all of the mass in the universe with the absorption clouds. Thus, although our results definitely confirm that gravitational lensing should produce a positive correlation between quasar luminosity and the number of absorbers, it appears unlikely that the effects of gravitational lensing are large enough to

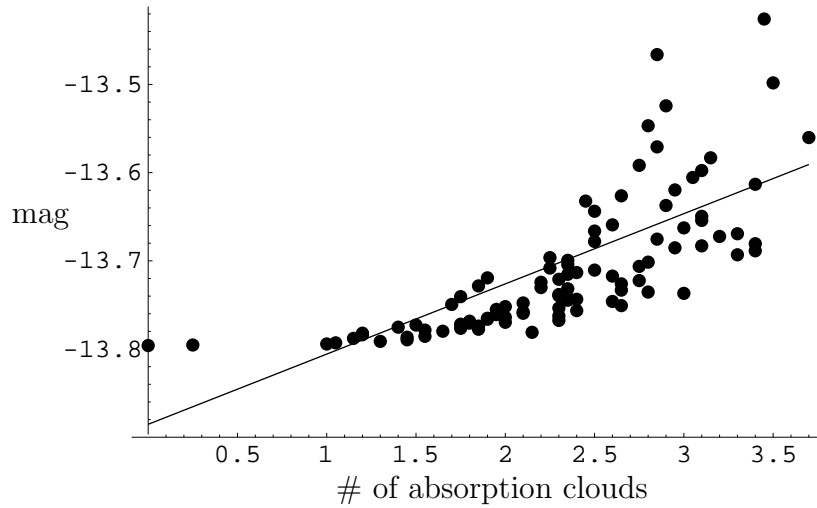


Figure 16: Magnitude vs. # of absorption clouds, for an $\Omega_0 = 0.1$, $\Lambda = 0$ universe, with galaxies treated as isothermal balls of mass $5 \times 10^{11} M_\odot$ and radius 50 kpc. The “magnitudes” are for (standard candle) quasars at redshift 2 (with an arbitrarily chosen absolute luminosity). The “number of absorption clouds” is the number of instances in which the photon beam passes through a galaxy in the redshift range $1 < z < 2$. The data is for 2,000 runs, and has been binned in groups of 20. The best fit line yields a slope of 0.08 magnitude per absorber.

explain the results of [1].

6 Lensing “Noise” and Bias in Measurements of q_0 Using Supernova Luminosities

One of the key goals of observational cosmology is to determine the parameters of what we have referred to as the underlying Robertson-Walker model of our universe, particularly the deceleration parameter, $q_0 = \Omega_0/2 - \Omega_\Lambda$ (where $\Omega_\Lambda \equiv \Lambda/3H_0^2$). Much progress has been made recently in this regard by using type Ia supernovae as standard candles [2]. The intrinsic dispersion of peak magnitudes of type Ia supernovae is of the order 0.2 magnitudes, and this number has been steadily decreasing with improved understanding of the phenomenology of type Ia supernova lightcurves. An important issue is whether or not lensing could produce a significant further dispersion of (distant) supernovae magnitudes. If so, lensing could be an important source of noise in estimates of q_0 . In addition, since the dispersion in luminosity produced by lensing is non-Gaussian and can be highly asymmetric about the mean—with a high probability for a small decrease in luminosity and a small probability for a large increase—lensing also could produce a significant bias in the results if there are selection effects or if the data is not properly analyzed. Indeed, using a Swiss cheese model to investigate this issue, Kantowski *et al.* [23] have claimed that lensing can have a large effect, causing a bias as large as 33% in q_0 measurements from supernovae at $z \sim 0.5$ when the true underlying Robertson-Walker model is one with $\Omega = 1$ and $\Lambda = 0$. However, using other methods, Frieman has recently argued that the induced flux dispersion in type Ia supernova magnitudes due to lensing is less than about 0.04 magnitudes for sources within a redshift of 0.5 [24]. If so, lensing would not, at present, be a significant source of noise, but might become important if the current intrinsic spread in type Ia supernova magnitudes can be halved through better understanding of the phenomenology of the light curves. Frieman’s estimates are consistent with those of Wambsganss *et al.* [15].

Our approach can be used to obtain the spread in image magnification (and, hence, amplification) of a standard candle at any given redshift, for any given cosmological parameters, and any choice of inhomogeneous distribution of matter. According to our conjecture in Subsection 3.4, randomly

distributed point masses should provide the most noise and/or bias, so it is particularly instructive to examine that case. Furthermore, as discussed in Sections 2 and 3, this case should provide a realistic description of lensing phenomena in our universe if most of the matter in the universe is clumped into stars.

Consider, first, the case of a universe with $\Omega = 1$ and $\Lambda = 0$ filled with randomly distributed point masses. A plot of area versus percentage of photon beams at $z = 0.5$ was previously given in Figure 2. We wish to convert this figure into a probability distribution for the apparent luminosity of a “standard candle” source randomly placed on a sphere of radius D centered on us, corresponding to $z = 0.5$. As we argued in Subsection 3.3, each source should have exactly one primary image. It is straightforward to obtain the probability distribution for the apparent luminosity of this primary image—and we shall do so below. However, as discussed in Subsection 3.3, we do not have a good way of determining which secondary images are associated with a given primary image, so we cannot directly obtain the probability distribution for the total apparent luminosity associated with a source. This is not a very serious problem in the present case, since Fig. 2 shows that less than 5% of the photon beams (as measured in the “present sky”) have undergone a caustic by $z = 0.5$, so that less than 5% of the total expected luminosity of the sources at $z = 0.5$ will be carried in secondary images. Undoubtedly, most of the luminosity carried by the secondary images will be associated with sources whose primary images are strongly lensed. Thus, if the primary and secondary images of a source cannot be resolved (as would be the case for microlensing by stars), the effect of including the secondary images should be merely to further brighten a few of the sources with the brightest primary images. Thus, the probability distribution we give below for the apparent luminosity of the primary images should be accurate for the total luminosity, except for the brightest sources.

To convert Fig. 2 to a probability distribution for apparent luminosity for the primary image of a randomly placed source, we proceed as follows. Let $p_z(A) dA$ denote the probability that a beam—which is randomly chosen with respect to the “present sky”—will have area between A and $A + dA$ at redshift z . Up to normalization, $p_{1/2}(A)$ is just the inverse of the slope of the curve plotted in Figure 2. Let $P_z(A) dA$ denote the probability that a source which is randomly placed on a sphere centered about us of radius D , corresponding to redshift z , will be “hit” by a beam with area between A and $A + dA$ which has not undergone a caustic. Then, as previously mentioned

in Subsection 3.3 above, we have

$$P_z(A) \propto A p_z(A). \quad (55)$$

Since the apparent luminosity, \mathcal{L} , of the source is proportional to $1/A$, the probability distribution, $\mathcal{P}_z(\mathcal{L})$, for apparent luminosity is given by

$$\mathcal{P}_z(\mathcal{L}) \propto \mathcal{L}^{-2} P_z(1/\mathcal{L}) \propto \mathcal{L}^{-3} p_z(1/\mathcal{L}), \quad (56)$$

where we have normalized both the beam area and intrinsic luminosity so that both A and \mathcal{L} would have unit value at redshift z in the underlying Robertson-Walker model. The probability distribution, $\mathcal{P}_{1/2}(\mathcal{L})$, is plotted in Fig. 17, using the data from Fig. 2 to determine $p_{1/2}(A)$.

It should be noted that, since at any z we have $p_z(0) \neq 0$, it follows from Eq. (56) that as $\mathcal{L} \rightarrow \infty$, we have at all z

$$\mathcal{P}(\mathcal{L}) \propto 1/\mathcal{L}^3. \quad (57)$$

Consequently, $\mathcal{P}(\mathcal{L})$ is normalizable (as it must be) and has a well defined first moment (since, as mentioned in Subsec. 4.2, the total expected apparent luminosity [including the secondary as well as primary images] must agree with that of the underlying Robertson-Walker model). However, its second moment is logarithmically divergent. As a result, the law of large numbers fails to apply to $\mathcal{P}(\mathcal{L})$. Thus, if one makes repeated measurements (by observing many supernova events) and averages the apparent luminosities, one will *not* obtain a sharply peaked Gaussian distribution about the average value. If the strongly lensed events are removed from the data sample, a Gaussian distribution would be obtained for the average value, but a bias will be introduced toward smaller apparent luminosity.

To obtain a rough, quantitative measure of both the “noise” and the potential bias in apparent luminosity measurements resulting from lensing, we inserted dotted lines in Fig. 17 to demarcate the upper and lower 16% of the probability distribution. If the probability distribution were a Gaussian, these lines would correspond to a “one sigma” error centered about the mean. Thus, the separation of these dotted lines gives a rough indication of the lensing “noise”, whereas the “off-centeredness” of the lines (away from 1) gives a rough indication of the potential bias that would occur if the strong lensing events were not included in the data sample. We see that in the point mass case, if the strong lensing events are excluded, the potential exists for a

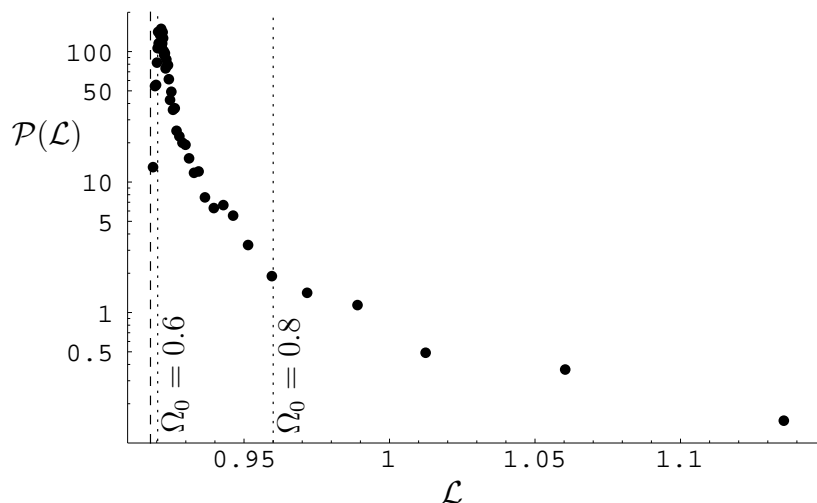


Figure 17: The probability distribution, $\mathcal{P}(\mathcal{L})$, for the apparent luminosity, \mathcal{L} , of a “standard candle” for an $\Omega = 1$, $\Lambda = 0$ universe with point mass galaxies, at a redshift of $1/2$. The absolute luminosity of the standard candle has been normalized to yield an apparent luminosity of 1 in the underlying Robertson-Walker model. The probability distribution shown is for primary images only; inclusion of the flux from secondary images presumably would mainly increase the luminosity of the most luminous primary images (which are off the scale of this plot), and should not significantly affect this figure. (Note that, according to Fig. 2, approximately 5% of the total luminosity is carried by secondary images.) The vertical dashed line represents the empty beam apparent luminosity, which is the minimum possible apparent luminosity for primary images. This empty beam apparent luminosity corresponds to a Robertson-Walker model with $\Omega_0 = 0.6$ and $\Lambda = 0$. The vertical dotted lines show the lower and upper 16% of this probability distribution, to give an indication of what one might roughly view as “one sigma” errors in this highly non-Gaussian distribution with infinite second moment. The Ω values corresponding to these lines also are shown.

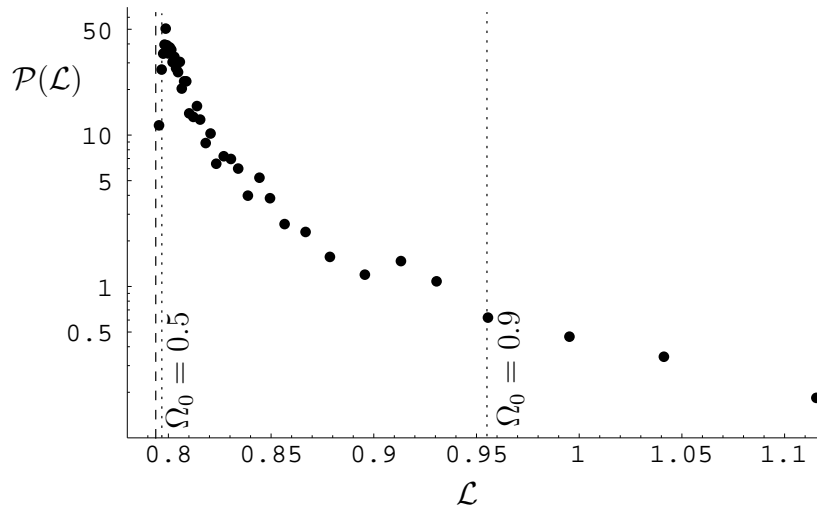


Figure 18: The probability distribution for apparent luminosity, \mathcal{L} , of a “standard candle” for an $\Omega = 1$, $\Lambda = 0$ universe with point mass galaxies, at a redshift of 1. The dashed and dotted lines have the same meaning as in Figure 17. Again, only primary images are considered. In this case, about 12% of the total luminosity is carried by secondary images (see Figure 3), so the corrections to the plot which would result from inclusion of secondary images may be somewhat more significant than in Figure 17.

significant bias toward values of apparent luminosity nearly as small as the empty beam value. This result is consistent with the results of Kantowski *et al.* [23], since the imposition of an “opaque radius” effectively excises the strong lensing events.

The corresponding plot at $z = 1$ for a universe with $\Omega = 1$ and $\Lambda = 0$ is shown in Fig. 18. As can be seen from this figure, both the noise and potential bias due to gravitational lensing are considerably larger at $z = 1$ than at $z = 1/2$. Figs. 17 and 18 appear to be in good qualitative agreement with the results of [12, 25].

The noise and potential bias due to lensing are considerably smaller if microlensing is not taken into account, as would be justified if most of the matter is smoothly distributed, rather than clumped into stars. As an example of a model with smoothly distributed matter, consider, again, the case of a universe with $\Omega = 1$ and $\Lambda = 0$, but now with the galaxies treated as

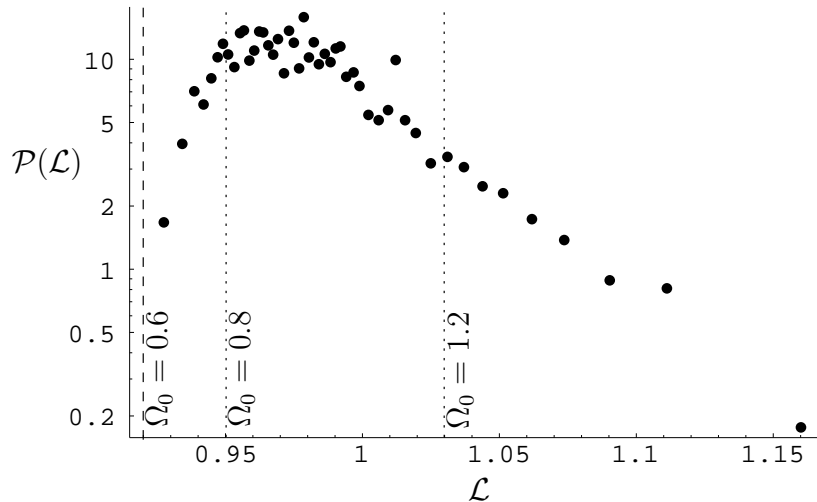


Figure 19: The probability distribution for apparent luminosity, \mathcal{L} , of a “standard candle” for an $\Omega = 1$, $\Lambda = 0$ universe with isothermal galaxies of radius 200 kpc, at a redshift of $1/2$.

isothermal balls of radius 200 kpc. The probability distribution $\mathcal{P}(\mathcal{L})$ for redshifts of $1/2$ and 1 are shown in Figs. 19 and 20. There are very few caustics even at $z = 1$ in this case, so the secondary images are of no importance. Inspection of Figs. 19 and 20 shows that the probability distribution is peaked much closer to 1 than in the point mass case, and the high luminosity “tail” of the distribution is much smaller. Thus, there would appear to be no significant danger of “bias” in this case. In addition, there is considerably less “noise” than in the point mass case. The noise estimate obtained from the dotted lines in Fig. 19 is in good agreement with the estimate obtained by Frieman [24].

Wambsganss *et al.* [15] have investigated a cosmological model with $\Omega_0 = 0.4$ and $\Omega_\Lambda = 0.6$ using a cold dark matter N-body computer simulation (normalized to COBE data) to determine the matter distribution. They studied lensing in this model and produced plots of $\mathcal{P}(\mathcal{L})$ at $z = 1/2$ and $z = 1$. It is instructive to compare their results with what would be obtained from our approach. To do so, we considered a $\Omega_0 = 0.4$, $\Omega_\Lambda = 0.6$ universe and distributed the matter in galaxies chosen to be isothermal balls of radius 200 kpc. (This choice of galactic mass distribution is merely our guess as to

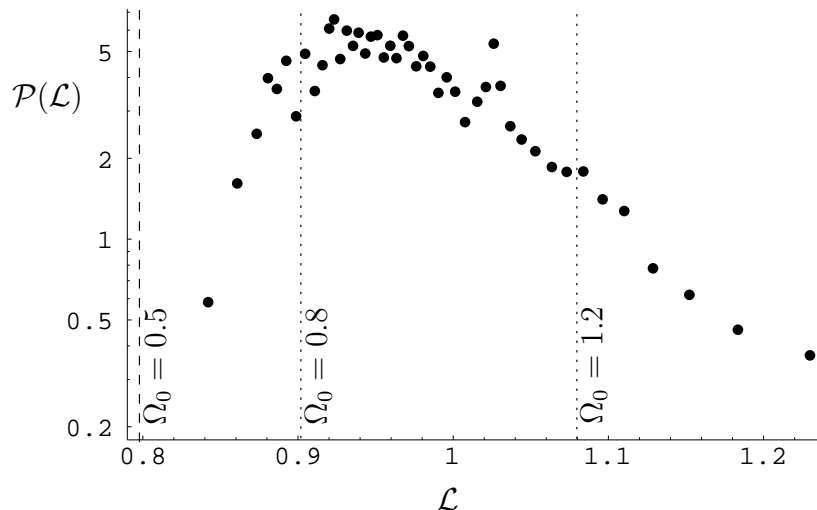


Figure 20: The probability distribution for apparent luminosity, \mathcal{L} , of a “standard candle” for an $\Omega = 1$, $\Lambda = 0$ universe with isothermal galaxies of radius 200 kpc, at a redshift of 1.

what should be reasonable for this cosmology; we did not attempt to match the results of the simulation used in [15].) In order to obtain good statistics for the comparison, we did 6,000 (rather than our usual 2,000) runs in this case. Our results for $\mathcal{P}(\mathcal{L})$ at $z = 1/2$ and $z = 1$ are shown in Figs. 21 and 22 respectively. Comparison with Fig. 1 of [15] shows very good agreement—apart from an overall normalization (which appears to have been chosen arbitrarily in [15]). Indeed, this agreement seems remarkably good in view of the fact that we did not attempt to adjust our galactic mass distribution to theirs, and, in our calculations, the clustering of galaxies is *not* taken into account. This latter fact lends support to the argument presented in Subsection 1.5 that, in almost all models, clustering of galaxies should have a negligible effect on the statistical distributions for magnification, shear, and rotation.

Finally, we note that a knowledge of $\mathcal{P}(\mathcal{L})$ over a range of redshifts contains a great deal of information about both the nature of the mass distribution in the universe and the parameters of the underlying Robertson-Walker cosmology. In particular, the shape of $\mathcal{P}(\mathcal{L})$ can be used to determine the fraction of matter in the form of condensed objects. We emphasize that, to do

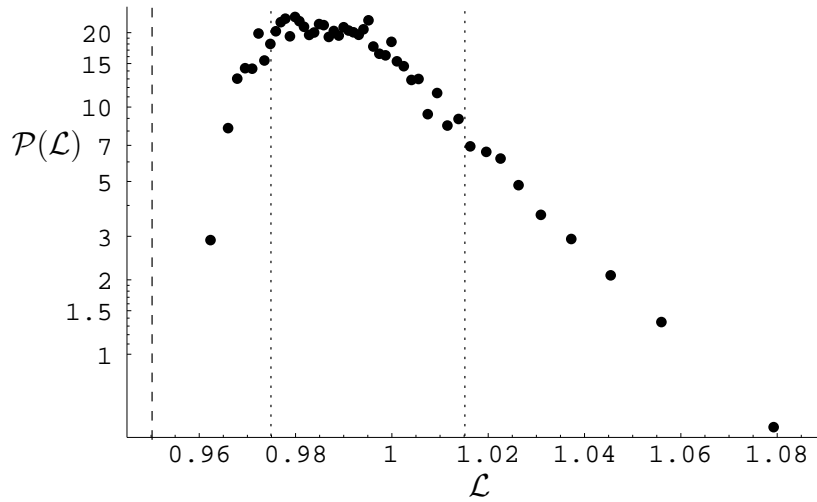


Figure 21: The probability distribution for apparent luminosity, \mathcal{L} , of a “standard candle” for an $\Omega_0 = 0.4$, $\Omega_\Lambda = 0.6$ universe with isothermal galaxies of radius 200 kpc, at a redshift of $1/2$.

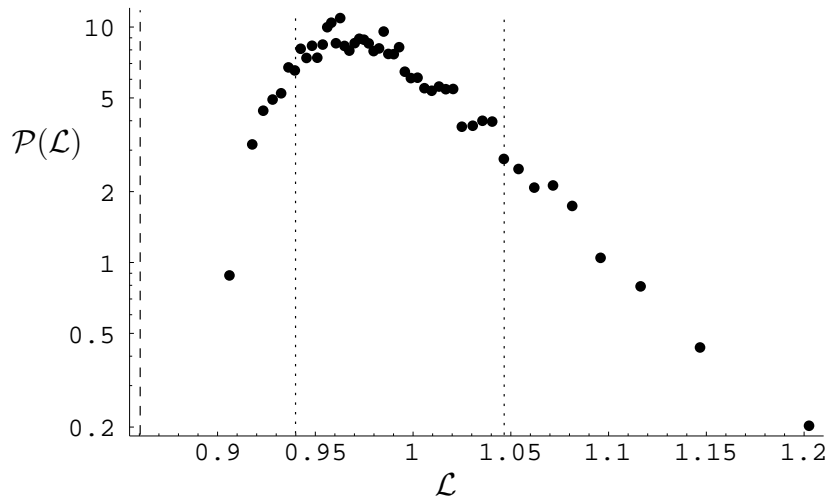


Figure 22: The probability distribution for apparent luminosity, \mathcal{L} , of a “standard candle” for an $\Omega_0 = 0.4$, $\Omega_\Lambda = 0.6$ universe, with isothermal galaxies of radius 200 kpc, at a redshift of 1.

so, it should not be necessary to go to the high luminosity tail of the distribution, as has been considered previously [12, 26], since there are considerable differences between, e.g., Figs. 18 and 20 at low apparent luminosities as well.

With regard to determining the parameters of the underlying Robertson-Walker cosmology, as indicated above, due to photon conservation the expected total luminosity—including both primary and secondary images—of all sources is independent of gravitational lensing effects. Thus, if no other sources of noise or bias are present, the apparent luminosity of a standard candle in the underlying Robertson-Walker model always can be obtained, in principle, by averaging the apparent luminosities of the observed sources. We stress that, since the probability distribution, $\mathcal{P}(\mathcal{L})$, can be quite asymmetric about its mean, it is crucial that one averages apparent luminosities rather than some function of them (like apparent magnitudes). Furthermore, in the point mass case—relevant if microlensing by stars is important—it will be necessary to make efforts to include the very bright images in the average in order not to bias the results toward smaller apparent luminosity.

Acknowledgements

The main stimulus for this work came from Don York, Dan Vanden Berk, and Jean Quashnock, who posed to us the issue of whether the results found in [1] could be accounted for by gravitational lensing. We wish to thank them for providing this initial stimulus and for many subsequent fruitful discussions. We also wish to thank Jürgen Ehlers for reading a preliminary version of this manuscript, and Éanna Flanagan and Josh Frieman for reading (nearly) final versions. Finally we wish to thank Eric Linder for giving a careful reading of the paper, and for many valuable comments. Our research was supported by NSF grant PHY 95-14726 to the University of Chicago.

References

- [1] D.E. Vanden Berk, J.M. Quashnock, D.G. York, and B. Yanny, *Ap. J.* **469**, 78 (1996), astro-ph/9605113
- [2] A. Goobar and S. Perlmutter, *Ap. J.* **450**, 14 (1995), astro-ph/9505022; S. Perlmutter *et al.*, *Ap. J.* **483**, 565 (1997), astro-ph/9608192

- [3] M.W. Jacobs, E.V. Linder, and R.V. Wagoner, *Phys. Rev.* **D48**, 4623 (1993)
- [4] T. Futamase and M. Sasaki, *Phys. Rev.* **D40**, 2502 (1989)
- [5] T. Futamase, *Mon. Not. R. astr. Soc.* **237**, 187 (1989)
- [6] R.M. Wald, *General Relativity*, University of Chicago Press (Chicago, 1984)
- [7] J.D. Jackson, *Classical Electrodynamics*, second edition, John Wiley and Sons (New York, 1975)
- [8] R. Kantowski, *Ap. J.* **155**, 89 (1969)
- [9] C.C. Dyer and R.C. Roeder, *Ap. J.* **189**, 167 (1974)
- [10] P. Schneider and A. Weiss, *Ap. J.* **330**, 1 (1988)
- [11] P. Schneider, J. Ehlers, and E.E. Falco, *Gravitational Lenses*, Springer-Verlag (New York, 1992)
- [12] K.P. Rauch, *Ap. J.* **374**, 83 (1991)
- [13] P.W. Premadi, H. Martel, and R.A. Matzner, *Ap. J.* **493**, 10 (1998), astro-ph/9708129
- [14] J. Wambsganss, R. Cen, and J.P. Ostriker, *Ap. J.* **494**, 29 (1998), astro-ph/9610096
- [15] J. Wambsganss, R. Cen, G. Xu, and J.P. Ostriker, *Ap. J.* **475**, L81 (1997), astro-ph/9607084
- [16] K. Tomita, *Prog. Theor. Phys.* **99**, 97 (1998)
- [17] C.C. Dyer and R.C. Roeder, *Ap. J.* **174**, L115 (1972); C.C. Dyer and R.C. Roeder, *Ap. J.* **180**, L31 (1973)
- [18] W.H. Press and J.E. Gunn, *Ap. J.* **185**, 397 (1973)
- [19] J.J. Dalcanton, C.R. Canizares, A. Granados, C.C. Steidel, and J.T. Stocke *Ap. J.* **424**, 550 (1994)

- [20] S. Seitz, P. Schneider, and J. Ehlers, *Class. Quant. Grav.* **11**, 2345 (1994), astro-ph/9403056
- [21] Y. Zhang, A. Meiksin, P. Anninos, and M.L. Norman, *Ap. J.* **495**, 63 (1998), astro-ph/9706087
- [22] Y.C. Pei, *Ap. J.* **440**, 485 (1995)
- [23] R. Kantowski, T. Vaughan, and D. Branch, *Ap. J.* **447**, 35 (1995), astro-ph/9511108
- [24] J.A. Frieman, *Comments Astrophys.* **18**, 323 (1997), astro-ph/9608068
- [25] Y.C. Pei, *Ap. J.* **403**, 7 (1993)
- [26] E.V. Linder, P. Schneider, and R.V. Wagoner, *Ap. J.* **324**, 786 (1988)